Development of Vibration Loading Profiles for Accelerated Durability Tests of Ground Vehicles

by

Ke Xu

A Thesis submitted to the Faculty of Graduate Studies of

The University of Manitoba

in partial fulfillment of the requirements of the degree of

MASTER OF SCIENCE

Department of Mechanical and Manufacturing Engineering

University of Manitoba

Winnipeg

Abstract

The accelerated durability test is an important part for design and manufacturing ground vehicles. It consists of test designed to quantify the life characteristics of a ground vehicle component under normal use conditions by testing the unit at higher stress levels to accelerate the occurrence of failures. The challenge of conducting accelerated durability tests is to create the driven profile. In general, the mission profiles of the accelerated durability test can be generated via the acceleration data of the events experienced by the vehicle during the field test. Accurately separating the time series signal that correlate the load events becomes essential to efficiently generate the mission profiles for the accelerated test analysis. The representative Power Spectrum Density (PSD) profile can be generated based on the mission profiles. Then, the driven profile for the sub-scaled accelerated durability test, i.e., the acceleration data can be generated based on the PSD data.

Acknowledgements

I would like to express my deepest gratitude to my advisor, Dr. Christine Q. Wu for providing me the guidance to carry out this work. This thesis would not have been possible without the help and support she has given me. I am grateful to her valuable suggestions and inspiration. I am grateful to Dr. Yan Wu's help for developing the mathematical methodologies for event identification. He has always made himself available to answering my questions patiently.

It is an honour for me to thank the committee members to help me to improve my work.

At the end, I would like to show my gratitude to my parents for all the support and for always believing in me.

Table of Contents

List of Figures

List of Tables

List of Symbols

PSD	Power Spectrum Density
ERS	Extreme Response Spectrum
SRS	Shock Response Spectrum
FDS	Fatigue Damage Spectrum
K	Stress to displacement factor
b	Fatigue parameter/Slope of S-N curve
C	Intercept of S-N curve
Q	Dynamic amplification factor
V_r	Variability of component damage resistance
Ve	Variability of environment damage
n_{test}	Number of tests to be undertaken on MAST
a'_{test}	Confidence level
k_c	Combined safety factor
k_t	Test factor
k_s	Safety factor
T_{full}	Full testing period
$T_{partial}$	Partial testing period

1. Chapter 1

Introduction

1.1 Background and Problem Statement

Safety and durability are important features for any product, especially for a ground vehicle. Ground vehicle customers are seeking a reliable and durable product that will last for many years. Ground vehicle testing ensures the product will meet customer expectations, and guarantee safety and comfort of the travelling public. For instance, to meet the durability requirements, one of the critical pre-launch requirements for the ground vehicles, such as motor coaches, is to pass the structural durability test on roads in-service. To verify the life time of various components, an equivalent mileage of millions of miles is required to be driven for the road test, which is extremely time and cost consuming. Therefore, field test is designed as the main portion of the test performed on a ground vehicle to represent the real world testing condition. During the field test, no mechanism failure including any crack initiation in critical suspension, frame and cab systems can be encountered.

The durability field test tracks are valuable to determine the durability and safety of the ground vehicles. The map of a typical testing facility for the proving ground field track test of Pennsylvania Transportation Institute is shown in Figure 1.1 [4]. There are many departments in the testing facility to evaluate the vehicles. The Vehicle Durability Test Track is used for the

vehicle's durability assessment. It contains different events that would simulate typical real world driving conditions.

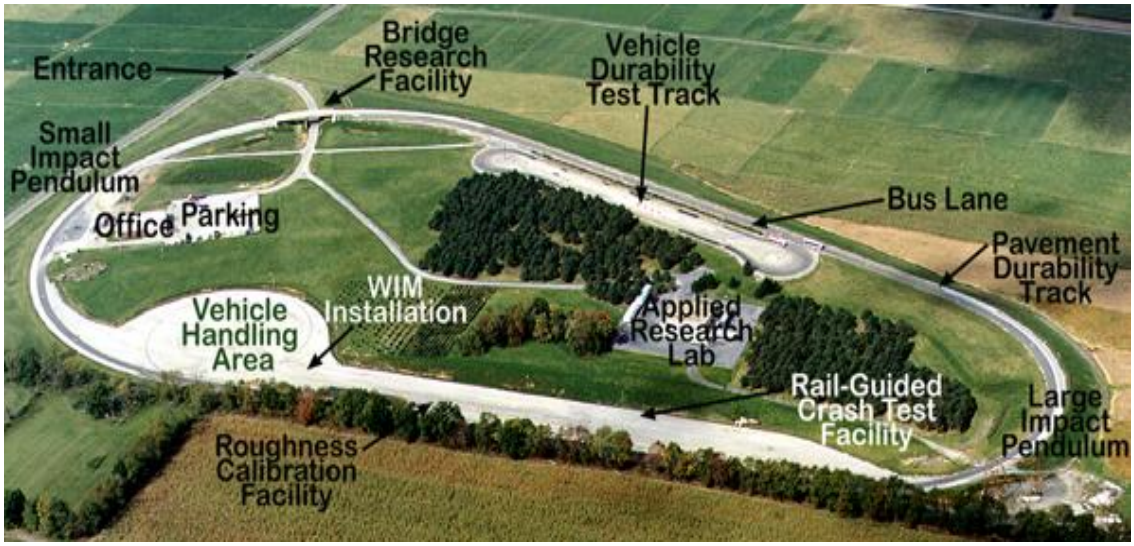

Figure 1.1: A typical testing facility for the automotive vehicles [4]

During testing, if any failure occurs an even greater time commitment would be required. Repeating the test is required once the problem is found and resolved [2]. The testing process is time and cost consuming. Therefore, a sub-scaled accelerated durability test is essential to ensure that the testing is completed in a timely manner [1]. A proficient accelerated durability test should satisfy the following two criteria:

1. The accelerated durability test should produce the same failure mechanisms as those observed in the real world loading conditions, i.e., being representative of the real loading environments.

2. The accelerated durability test should be accelerated while no occurrence of the unrealistic high load which can possibly alter the failure mechanisms.

Hence, the possible failure components can be found using the accelerated durability test before the field test, and the vehicle's performance can be evaluated within a much shorter time. At the

same time, the results of accelerated test should reveal the same potential damage content as the product would encountered over its service life. Other important information such as the determination of the warranty timeframe and minimization of product recalls and complaints after market can be obtained once the accelerated durability test is conducted [1].

The accelerated durability test is carried out by the use of Multi-axis Simulation Table (MAST). Other important applications of MAST include the noise and vibration test and performance evaluation. MAST is a mechanical system that works in a controlled laboratory environment by repeatedly replicate and analyze “in service” vibrations and motions of a testing component [59]. The MAST has a six degree of freedom control system; it provides the mounting surfaces for the testing component analysis. This MAST operated through the uses of the hydraulic actuator and advanced flex test controller. In addition, different forms of data such as sinusoidal, random Power Spectrum Density (PSD), swept sine wave can be taken as the input of the MAST. Many advantages of the lab test comparable to the field test includes: individual test component can be tested instead of the whole system, the testing time and cost commitment are significantly low, the modification of the road profiles for the field test can be conducted [60].

As a result, it is highly desirable to conduct accelerated durability test in a lab for ground vehicles components. The prototype of the MAST that is used for the sub-scaled accelerated durability test is shown in Figure 1.2:

Figure 1.2: WESTEST's MAST table [3]

The MAST that implements the accelerated durability test can be directly driven using the acceleration time series format data [2]. As a result, the driven profile of acceleration data with shorter duration needs to be created to implement the actual test on MAST, which is a crucial part of developing accelerated durability tests.

1.2 Literature Review

Accelerated testing consists of tests designed to quantify the life characteristics of a ground vehicle component under normal use conditions by testing the unit at higher stress levels to accelerate the occurrence of failures. The challenge is to create the driven profile for MAST. Commercial GlyphWorks software has been developed to create such a driven profile. There are two essential tasks to generate the accelerated loading profile using GlyphWorks: (1) creating the mission profile, and (2) developing the accelerated loading profile. Once the driven profile is

generated, it can be further used for the durability assessment of test component either experimentally or numerically.

1.2.1 Accelerated Durability Test

Traveling during the service environment, dynamic loads act on the complete vehicle through the roughness of the road, and subsequently on the subsystems, and finally yield local stresses and strains which cause fatigue and failure. Accelerated durability test is to test ground vehicles or their components under the dynamic loads. Therefore, the repetitive load on the substructure or the component needs to be produced, causing an equivalent stress level and subsequently lead to the same cumulative damage for the structure failure with a shorter duration. A representative loading profile for both of the design and the testing is essential to predict the service life; its determination is a difficult and vital task. In general, there are two different types of loads to simulate the service loading environment: sinusoidal loading and random loading, in which different rules are governing the relations between the stress cycles during the test and service environment [45]. The input random loading profiles are generally the accelerations, displacements, forces or strains. An example of input load measurement is introduced by Gopalakrishnan and Agrawal [62]. The measurement of tri-axial wheel forces, including the vertical, longitudinal and lateral is made using load-cell that is attached to the wheel hub. When the measurements approach is not practical, the dynamic input load can be established using Multi-body dynamic simulation technique as an alternative [62].

In the automotive industry, there are two approaches used for the accelerated durability assessment once the loading profile is generated. The first approach is the numerical technique and the second approach is the physical testing of the prototypes, for the same objectives of

shorten design cycle time, and reduce development cost. In each approach, many methods have been developed in the literature, especially in the numerical approach.

Limited experimental accelerated durability assessment methods are available in literature. Two systematic ways are generally used for the experimental accelerated durability assessment [61]. The first common method is to use special field test tracks that are designed to allow the vehicle to travel under the same load as the public roads within a much shorter time. However, to derive a relation between the loads between the public roads and the loads from the test tracks becomes a difficult task. The second method is to bring the test into the laboratory based on the serve-hydraulic test rigs. The benefits of this method is the test can be better reproduced and observed, as the individual testing component is tested under the controlled environment other than the full vehicle prototype. However, the challenge exists as the loads to be used in the rig test have to be derived based on the measurements performed either on the test tracks or the public roads [61]. An example of the driven profile development for the accelerated durability test is demonstrated in [64]. Xu presented a technique for developing a high accuracy laboratory durability test of a light-duty pickup truck on a six degree-of-freedom road test simulator (RTS) [64]. The road data acquired from the proving ground was used for driven file development on a RTS, for the subsequent accelerated durability test. Various transducers were instrumented on the vehicle under studied. Therefore, the data of vehicle wheel forces and moments, spindle accelerations, spindle to frame displacements, loads at cab and cargo box mounts, and frame strains and rear axle torsion were measured. Five vehicle response control channels configurations were used. Subsequently, the correlation of transducer responses between those achieved on the RTS and the road data were compared. The configuration that produced the best correlation with proving ground responses was adopted to develop the final accelerated test driven files in the lab,

meanwhile, the configuration provided guidance for the instrumentation of testing specimens [64, 67].

An overview of numerical methodologies for durability assessment of the ground vehicles is detailed in [63]. Generally, there are three steps involved for the numerical durability assessment process. They are the determination of the load input, stress analysis and fatigue analysis. The load input is obtained either from measurements or simulations. The stress analysis can be preceded based on the input load. Finally, the fatigue analyses can be conducted based on the stress or the strain analysis to predict the fatigue life. Each of the three stages involves many methods.

The methods of stress analysis used for the durability assessment are developed either in the time domain or in the frequency domain. Methods available in the literature are quasi-static finite element analysis, co-variance method, eigenvalue finites element analysis, etc. [63]. In different stress analysis methods, different algorithms are employed for the stress level determination, and the choice of the algorithm depends on the type of input load.

Finally, methods have been developed for the fatigue analysis. Popular ones includes Cycle Counting [65], Stress-life approach, strain-life approach [66], fracture mechanics approach [63]. As demonstrated by Wannenburg and Heyns, the preferred method that is universally adopted in the automotive industry is the strain-life method due to its advanced theoretical background. In the case of heavy vehicles, where the welding failure dominates the failure mechanisms, the stress-life method is preferred [63].

In this work, an experimental approach is developed for the driven profile generation of sub-scaled accelerated durability test, based on the commercial Glyphwork software.

1.2.2 Accelerated Durability Test Development Using GlyphWorks Software

GlyphWorks, developed by HBM nCode, is a computer software package with multi-file, multi-channel, multi-format environment. It uses for power processing and engineering test data analysis, with specific application to durability assessment and fatigue analysis [1]. The driven profile of sub-scaled accelerated durability Lab test conducted in this project is generated using this commercial GlyphWorks software.

Using GlyphWorks, the important accelerated durability test profiles can be best achieved by using a so called ‘Mission Profiling and Test Synthesis’ processes. Mission Profile comprises a number of load events that simulate the real world driving conditions, containing dynamic loading information about the vehicles. Fatigue damage content and shock response of each individual event are the output of the Mission Profiling process. Test Synthesis is accomplished along with the information about the recurrence of the events expected in the field test. A synthesized accelerated test PSD can be created using the Test Synthesis process. The accelerated durability test with the desired test period is called the full-period accelerated durability test. However, the corresponding PSD data of the full-period accelerated test cannot be practically applied in the lab due to required tuning of each actuator. Therefore, the generation of the vibration load for a shorter time period which contains major features as the full-period accelerated test is required. The driven profile with required shorter time duration is defined as the loading profile of partial-period accelerated test. It can be directly applied to the sub-scaled accelerated test on MAST. The driven profile in terms of acceleration data for the partial-period test can be created based on the Custom Fourier process under GlyphWorks using PSD as the input.

1.2.3 Events Identification

One of the challenges of using Glyphworks is to generate the mission profiles, which can be efficiently created using the acceleration data of corresponding events experienced by the vehicles. Therefore, events identification is the first essential step to effectively conduct the accelerated durability test. Initial developments of events identification includes the visual identification method and the curve fitting method [6, 7], but with limited success. In the visual identification method, many assumptions and approximations have been proposed, affecting the accuracy of the identification results [6]. With the curve fitting method, only few events can be identified from the counter-clockwise data of the field test [7]. In addition, no previous studies have been done to develop a systematic and robust events identification approach from the field test data to effectively generate the mission profiles for the accelerated durability test. Motivated by this point, a method to identify the events from the acceleration field test data automatically and accurately is developed in this work, which is based on wavelet analysis, clustering, and Fourier analysis.

1.2.3.1 Wavelet Analysis

Wavelet analysis is originated from the beginning of the 20^{th} century [8]. The modified and advanced versions are available nowadays for applications in many areas, such as data mining and system denoising. Moreover, the wavelet analysis has been used as a new and advanced technique for dealing with various signals, including time series. In wavelet signal processing, important applications, including signal encode, decomposition, reconstruction, and simplification have been greatly encountered in the literature. In addition, wavelet signal processing becomes an enormously important and influential mathematical tool for application in

another field of signal denoising. According to the literature, statistical method, Fourier transform and wavelet transform are the main methodologies available for the purpose of noise removal from the noisy signals. Depending on the type and the character of the noisy signal, the noise can be reduced either in the frequency domain or directly in the time domain [9]. The method of noise reduction progressed in the frequency domain can be accomplished by the uses of the discrete Fourier transform, and it can be preferably used when both of the noise and the signal have stationary trends. The limitation comes from the fact that no corresponding time information is available on when the important frequencies occurred. Alternatively, the short Fourier transform can be applied as a compromise between the time resolution and the frequency resolution, mapping a signal into a two dimensional functions of time and frequency. However, better resolution in one field often results in a poor resolution in another, as once the particular size for the time window is fixed; it is the same for all frequencies [10, 11]. Then, a more advanced alternative of wavelet transform can be used for the purpose of denoising; more precise information on both of the low and high frequencies domains can be determined. The wavelet analysis uses a time-scale domain instead of time-frequency domain [10]. As a result, signal with non-stationary data can be better handled [11]. In addition, the transform domain denoising is believed easy to separate the noise energy from the main one. Therefore, wavelet transform is selected as the method to denoise the acceleration signal in this work.

Wavelet denoising can be accomplished by the uses of Wavelet Toolbox, a tool for analysis and synthesis signals with collection of functions built on the MatLab environment. In Wavelet Toolbox, both of the command line functions and graphical interactive tools are available for the analyzing and the synthesizing of signals. Both of the one-dimensional and two-dimensional signals can be analyzed using the multipurpose tool of Wavelet Toolbox. Acceleration time

series is a one dimensional signal that can be processed for the purpose of noise removal in Wavelet Toolbox.

1.2.3.2 Clustering Method

Clustering methodologies have been successfully applied in the fields of engineering, computer science, economics, astronomy and earth science [12]. In engineering applications, pattern recognition based on clustering becomes increasingly important; as well as machine learning. As listed in [12], a number of 200 major subject categories in clustering have already been developed in the past decade. Referring to [12], many existed clustering algorithms are pattern recognition dependent.

There are many clustering definitions available in the literature. An original definition is given by Backer and Jain [13], “in cluster analysis a group of objects is split up onto a number of more or less homogeneous subgroups on the basis of an often subjectively chosen measure of similarity, such that the similarity between objects within a subgroup is larger than the similarity between objects belong to different subgroups”. One of the other definitions available in the literature described as [12], “clusters may be described as continuous regions of this space (d-dimensional feature space) containing a relatively high density of points, separated from other such regions by regions containing a relatively low density of points.” The clustering algorithm designed for this project is based on the clustering definition, defined as: “a cluster is an aggregate of points in the test space such that distance between any two points in the cluster is less than the distance between any point in the cluster and any point not in it” [12]. Some general clustering algorithms available in the literature contain Hierarchical clustering, Patitional clustering, Neural Network-based clustering, Kernel-based clustering, Sequential Data

clustering, etc. Generally, the clusters are classified based on the similarity or the dissimilarity using the proximity measures [12]. Within each clustering algorithm, different clustering strategy and proximity measure methods are adapted [12]. Most specifically, problem dependent definition can be given to the proximity measure based on the character and feature type of the data, and the measurement level [12]. Clustering is a subjective and problem-dependent process [12]. For instance, in the same clustering algorithm, with different parameters chosen, different clustering results could be obtained.

There are three clustering algorithms specifically used to deal with the time series data. The raw-data-based approach is introduced to directly deal with the raw data. The feature-based approach is used to indirectly deal with the features extracted from the raw data. The model-based approach that is used to indirectly deal with the models built from the raw data [14]. Different clustering algorithms, similarity and the dissimilarity measures, and evaluation criteria are defined for each of the clustering methods [14]. The first approach is designed to specifically deal with the multivariate time varying data, the second approach is used to manage the raw data with high-dimensional space, and the last approach is used to deal with the time series that are built within different models. However, all the existed clustering algorithms cannot be applied for the purpose of events identification in this work, as the distance measures for the known cluster algorithms require large volume of data, while our data are small in size. Therefore, we have to find new ways for cluster identification. Extracting spectral contents off time series does not require a lot of data points. That is why we are using peak-to-peak gaps as a measure for clustering purpose effectively in the time domain.

1.2.3.3 Fourier Transform Analysis

Fourier transform is a popular mathematical operation to analyze a signal by decomposing it from its time domain into the frequency domain. The Fourier transform analysis is popular in areas of signal processing and signal recognition.

Many generations of the Fourier transform have been applied for various types of signals. For example, in the biomedical signal processing applications, the Fourier transform has been used as a time-frequency analysis on families of biomedical signals (e.g. EEG, EMG). Additionally, the time-frequency map in the Running Discrete Fourier transform analysis is used to recognize different types of waveforms, e.g. waveforms of alpha, theta and delta in EEG signal. Also, the frequency components of muscular contractions can be categorized in EMG signals. In addition, the time-frequency map offers as an excellent tool to compress the biomedical data, coding the information exceeding the noise level [15].

A new optimal approach of one- or multi- dimensional Fourier transform used for pattern recognitions has been presented by Gelman and Braun [16]. Both of the real and imaginary components of Fourier transform can be simultaneously used as recognition features, this approach can specifically deal with the Gaussian stationary zero mean signals.

The Fractional Fourier transform (FRFT) as a generalization of the Fourier transform has been developed. One of the practical applications of FRFT time–frequency based representations is speech and music processing. Increasing applications in the area of mechanical vibrations analysis can be found in the literature. However, it is demonstrated that the FRFT time–frequency tool cannot provide a sufficient framework for a comprehensive analysis [17]. In addition, the traditional applications of the FRFT include filtering and signal recovery, watermarking and communications have been introduced [18]. In spite of many applications, the

Fourier transform has never been applied to a time series data for events refinement purpose based on a frequency analysis.

1.3 Objectives

To generate the input load profiles for the sub-scaled accelerated durability test using MAST, two main portions need to be completed independently in GlyphWorks. The first portion is to generate the representative PSD profile for the accelerated durability test. The second portion is to generate the durability acceleration driven profile for the MAST. The mission profiles can be generated using the corresponding events data of the field test. The PSD profile can be generated based on the mission profiles. Then the input loading profile can be generated using the representative PSD data. Therefore, the challenges of this work lie in two phases. First, to accurately identify the field test events for their correlated data is very difficult. Second, there is no constructive approach to accurately generate the accelerated durability test PSD profiles. Correspondingly, there are four objectives for this work.

1st objective: to develop an approach on how a time series can be separated and correlated into its component events by using an automatic and robust method. An approach consist of three mathematical methodologies is developed; they are the wavelet analysis, clustering algorithm, and Fourier analysis.

2nd objective: to provide a systematic approach to generate the PSD profile of the full-period accelerated durability test from the mission profiles, which can be created using identified events data using the GlyphWorks software. In addition, to implement the generated full-period PSD data, driven profile of the partial-period test needs to be further created.

3rd objective: to introduce systematic approaches for the driven profile generation and validation processes for the partial-period test. Furthermore, certain parameters have significant effects on the loading profiles generation for a valid partial-period test.

4th objective: to analyze the effects and study the sensitivity of the key parameters on the quality of important accelerated test profiles, parametric analysis is carried out.

Methods used to describe the events identification based on the wavelet method, clustering analysis and Fourier analysis are presented in Chapter 2. Methods related to the accelerated durability test conduction using the extracted events data of the field test will be detailed in Chapter 3. The methodologies used for generating the accelerated durability test mission profiles are shown in section 3.1. In section 3.2, the method for generating the full-period accelerated durability test PSD profile will be presented. To implement the full-period PSD profile, method of generation the partial-period accelerated durability test is detailed in section 3.3. Then the validation process of the partial-period test is shown in section 3.4. In addition, parametric analysis on the important profiles of the accelerated durability test will be studied in section 3.5. In Chapter 4, results of events identification, mission profiles, PSD profiles, and driven profiles of the accelerated durability test, and the parametric analysis of important parameters will be shown along with discussions. Finally, conclusions are drawn in Chapter 5.

2. Chapter 2

Development of an Approach to Event Identification Using Field Test Data

In general, the mission profiles of the accelerated durability test can be generated via the acceleration data of the events experienced by the vehicle during the field test. The representative PSD profile can be generated based on the mission profiles. Then, the accelerated durability lab test driven profile, the acceleration data can be generated based on the representative PSD data. The mission profiles, PSD profile, and driven profile for the sub-scaled accelerated durability test are generated using the commercial GlyphWorks software. The challenge of accurately separating the time series signal that correlate to the load events becomes essential to efficiently generate the mission profiles for the accelerated test analysis. An approach, which can automatically identify the events embedded in the acceleration time series is developed in this chapter.

2.1 Field Test Events and Time Series Information

The set of the field test time series used to identify the events and generate the accelerated vibration driven profiles are accelerations collected from the proving ground field track test at Pennsylvania Transportation Institute [4] as shown in Figure 1.1. There are seven events

contained in a typical field test track that are separated into two sections: the three-event section and the four-event section, as shown in Figure 2.1:

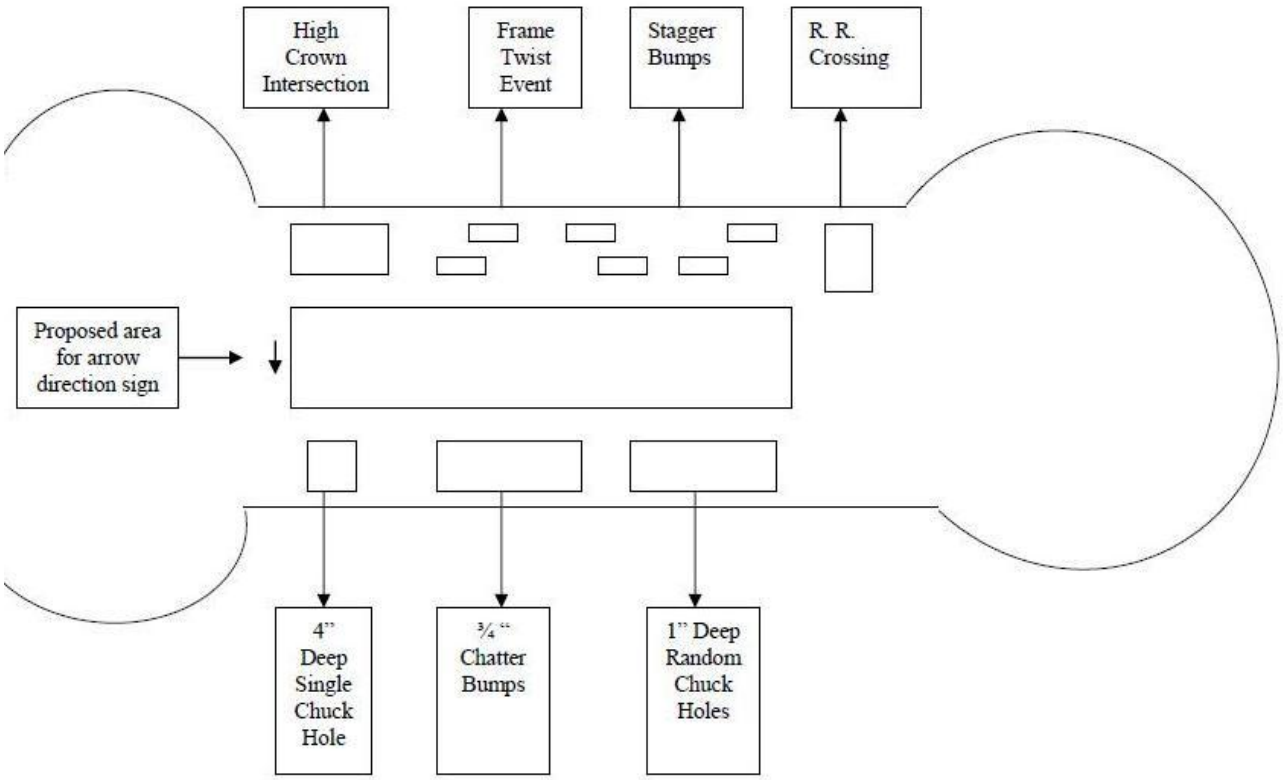

Figure 2.1: A typical field test track for motor coaches [4]

As shown in Figure 2.1, two transitions can be observed between the three-event section and the four-event section. The field test duration is 650 hours including both of the transitions and event sections, and 330 hours are for the event sections. The measured travelling speeds of the vehicle on the test track for each event is shown in Table 2.1:

Table 2.1: Measurement of the travelling speed for each of the seven events of the test track

	Event Name	Speed of the vehicle
Event 1	4" Single Chuck Hole	5mph
Event 2	3/4" Chatter Bumps	20mph
Event 3	1" Random Chuck Holes	20mph
Event 4	Railway Crossing	8mph
Event 5	Staggered Bumps	10mph
Event 6	Frame Twist	10mph
Event 7	High Crown Intersection	10mph

The estimated durations of each event can be calculated based on the driving speed given in Table 2.1, and the information about events geometries, as shown in Figure 2.2(a)-(e). The estimated duration of each event will be used to demonstrate the effectiveness of the proposed event identification approach to correlate the acceleration data with the corresponding events.

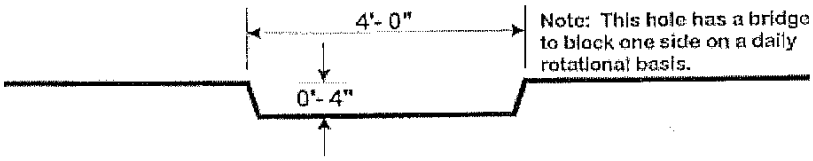

(a)

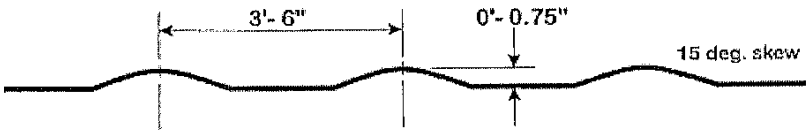

(b)

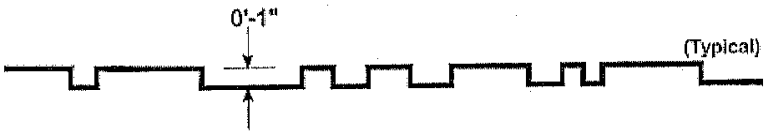

(c)

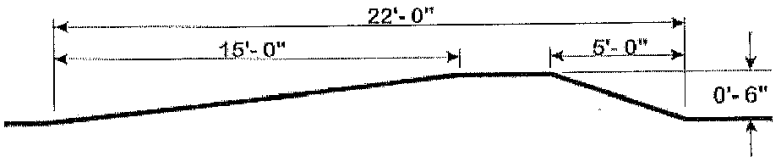

(d)

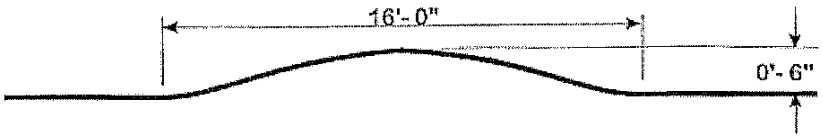

(e)

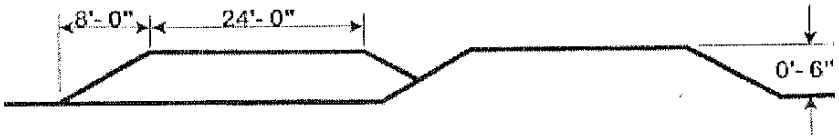

(f)

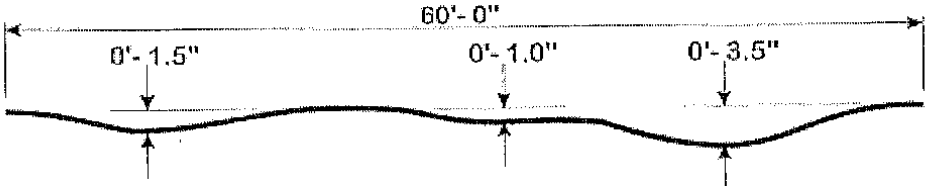

(g)

Figure 2.2: Event Geometry of (a) 4'' Deep Chuckhole (b): 3/4" Chatter Bumps (c) 1" Random Chuck Holes (d) Railway Crossing (e) Staggered Bumps (f) Frame Twist (g) High Crown Intersection

The collected acceleration data used for the events identification includes three counter-clockwise laps followed by three clockwise laps, and each lap contains seven transient events, as shown in Figure 2.1. The X and Z represent the longitudinal and the vertical directions of the vehicle. The accelerations in X and Z directions will be used for the events identification, as shown in Figure 2.3. The horizontal axis is the time in the unit of second, and the vertical axis is the acceleration in the unit of g.

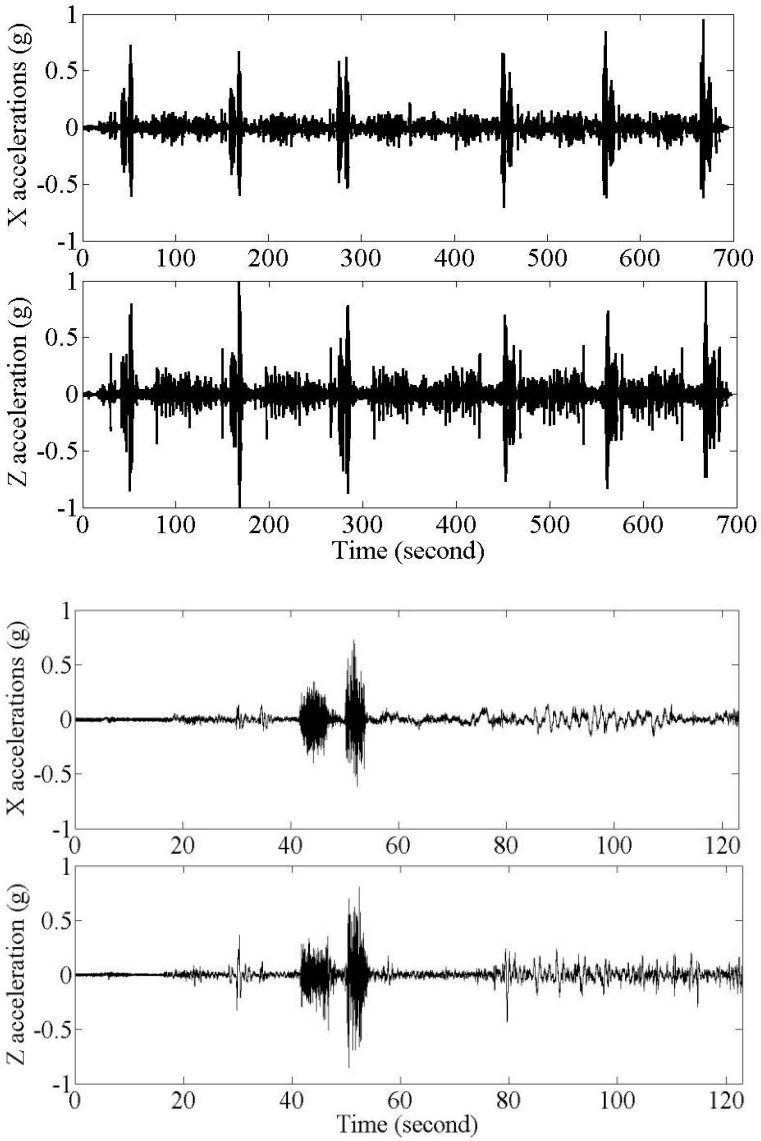

Figure 2.3: Acceleration data measured from the field tests in X, Z directions (a) for 6 laps (b) for 1 lap

Referring to Figure 2.3(b), the seven events, as shown in Figure 2.1 are contained in each lap of the time series. The corresponding time instances of the start and the end of each event need to be identified. An event identification approach is developed here. The proposed approach consists of three parts; (1) the wavelet transform method, (2) the clustering analysis, and (3) the Fourier transform analysis. The wavelet transform method is introduced to denoise the acceleration signal. A new clustering algorithm is designed here to identify the seven events. Then, the Fourier transform analysis used as a frequency based analysis is developed to refine the segmentations of the initial clustered events. The whole events identification and refinement processes are summarized in Figure 2.4:

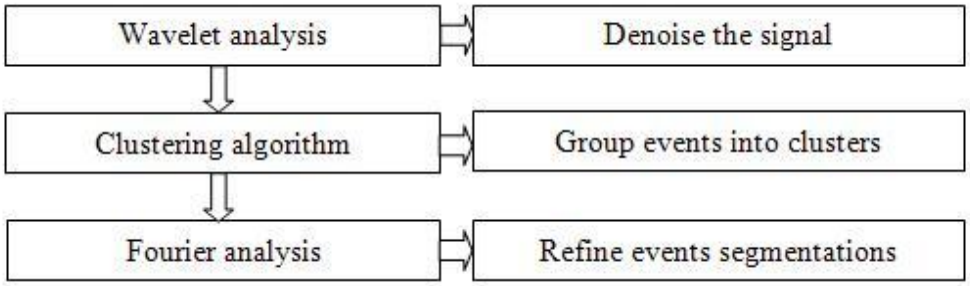

Figure 2.4: Proposed frame work for the events identification approach

In the following subsections, methods of wavelet transform analysis, clustering algorithm, and Fourier analysis will be shown, respectively.

2.2 Denoising Acceleration Signal Using Wavelet Analysis

Different signals may be contaminated by the additive noise due to various reasons depending on the processes of collecting and processing data. The possible reasons of the noise production in the acceleration signal during the field test are due to the characteristics of road structures during the transportation, the requirements of different travelling speed, the measurements of

acceleration data using accelerometers, the vibrations of the engine and suspension systems, and driving behaviour and meteorological conditions, etc. Generally, denoising is a process to remove the additive noise, while the characters or the features of the signal are retained as much as possible [19]. Denoising is an essential step before analysing signals. Most importantly, it is believed that denoising not only has effects on the clustering result, but also speeds up the data processing [8]. Generally, there are three steps involved in accomplishing the wavelet denoising process, which is summarized in [10]:

(1) Decomposition: the acceleration signal is decomposed into multi-levels of resolution in the levels of wavelet coefficients via the Discrete Wavelet Transform (DWT).

(2) Noise removal: some wavelet coefficients are chopped using a thresholding technique. Usually, those coefficients correspond to high frequency contents related to noise.

(3) Reconstruction: the Inverse Wavelet Transform (IWT) operation is performed using the thresholded wavelet coefficients, and then the denoised signal is reconstructed.

The wavelet denoising process is accomplished using the Wavelet Toolbox [22], a computer software used to analyze and synthesize signals in MatLab. The denoising procedure is summarized as follows in Figure 2.5:

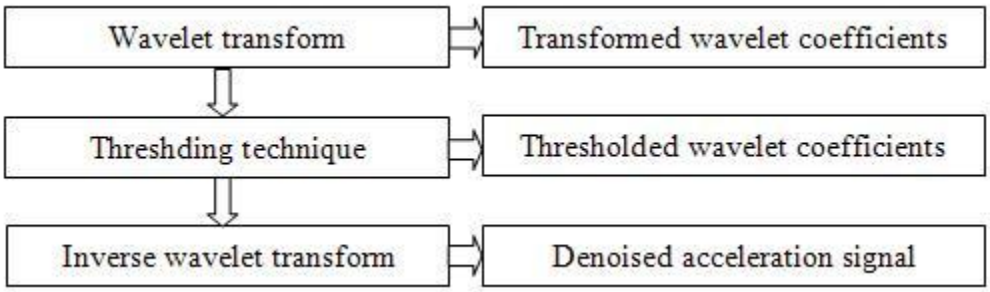

Figure 2.5: General wavelet denoising procedure

Referring to Figure 2.5, the detail discussion of each step is presented in the following subsections.

2.2.1 Discrete Wavelet Transform (DWT)

Implementation of the DWT leads to the algorithm of filtering operation. The wavelet coefficients are derived by passing a signal through the filters [20]. The low pass (LP) and the high pass (HP) filters are utilized for this filtering process. The decompositions from LP filter are named as the approximation; and those from the HP filters are the detail. The approximation contains the high-scale and low-frequency components. On the other hand, the detail contains the low-scale and high-frequency components of the signal.

From an energy viewpoint, the low-frequency component, represented by the large coefficients reveals the main feature of the signal because it usually contains the important information. Conversely, the high-frequency components, corresponding to the small coefficients are more likely due to the presence of the noise [19]. Therefore, to further analyze the signal the insignificant coefficients need to be removed.

Both of the wavelet analysis and the wavelet packets analysis are available for the filtering process. They are differentiated by the format of splitting. The process of splitting repeated on the approximations side to produce different levels of the approximations and the details using LP filters and HP filters is called wavelet analysis. Additionally, wavelet packets analysis exists as an extension of the wavelet analysis. It decomposes both of the approximations and the details using the LP filters and HP filters to produce multi levels of approximations and details. The flow charts of levels of decomposition processes for both of the wavelet analysis and the wavelet packet analysis are shown in Figure 2.6 and Figure 2.7, respectively:

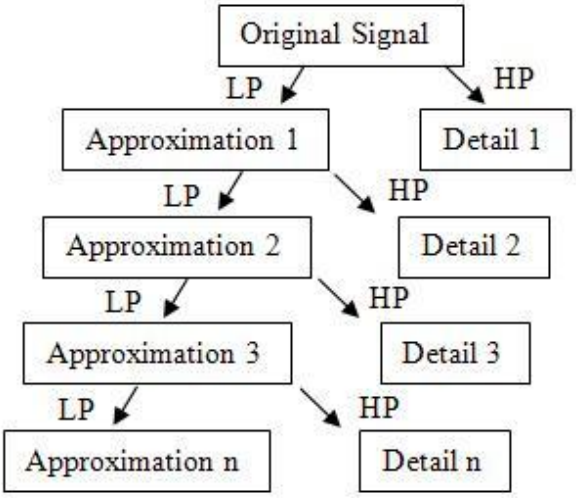

Figure 2.6: Levels of decompositions for the wavelet analysis

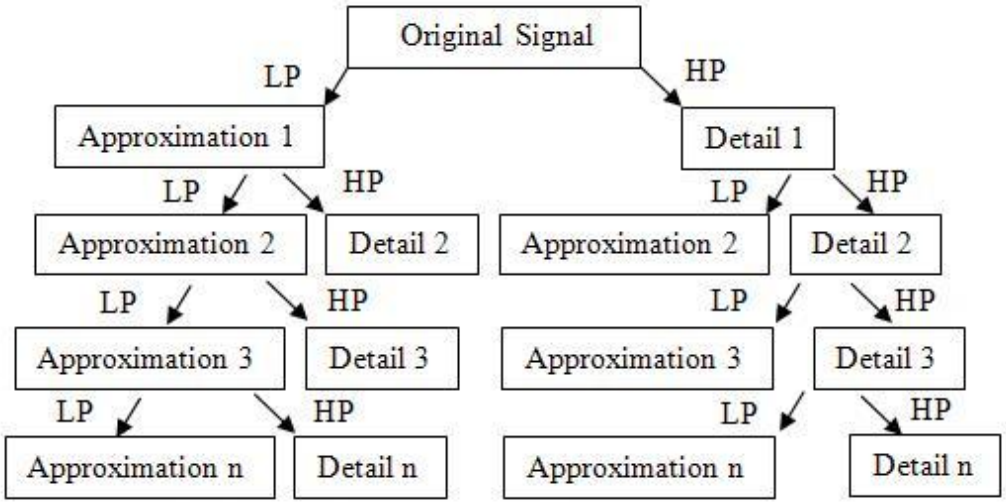

Figure 2.7: Levels of decompositions for the wavelet packet analysis

Referring to Figure 2.6 and Figure 2.7, the wavelet analysis will speed up the denoising process versus wavelet packet analysis. The approximations are believed to contain the important information; therefore, the wavelet analysis instead of the wavelet packets analysis is preferred in this project. Both of the wavelet analysis and wavelet packet analysis are built within the Wavelet Toolbox.

The proper level of decompositions selection is essential to capture significant acceleration spikes, as shown in Figure 2.3(a); consequently, the important information will not be lost. There are criteria for the wavelet level selection. As discussed in [4], the maximum level of decomposition to be applied to the wavelet coefficients relies on the number of available data points and the level of the signal to noise ratio (SNR) of the original signal. SNR is defined as [35]:

$$SNR(dB) = 10\,log(S_{signal}/S_{noise}) \tag{2.1}$$

where S is the root mean square (rms) power of acceleration signal and the additive noise. Generally speaking, the denoisd signal needs to have a higher value of SNR comparing to the original signal. In addition, there is no such a single type of wavelet can be applied for various denoising applications. Different wavelets should be applied for denoising different types of signals, and different levels within the same wavelet family can be further selected.

2.2.2 Wavelet Coefficients Thresholding Methods

The next step to accomplish the noise removal process is thresholding; it is a non-linear technique operating on the wavelet coefficients [19]. The wavelet coefficients that correspond to the low frequency information need to be retained. There are many thresholding methodologies available. The two general algorithms available for thresholding the wavelet coefficients are the soft thresholding and the hard thresholding. Both of the thresholding techniques are built on comparing the transformed coefficients against the predefined threshold value. Hard thresholding sets zeros for all wavelet coefficients whose absolute value is less than the specified threshold limit, and retains the remaining coefficients unchanged. The hard thresholding technique is

defined in Equation (2.2); the transformed coefficients is denoted as x, the predefined threshold value is denoted as λ, and the thresholded coefficients denoted as $T_{hard(x)}$ [24]:

$$T_{hard(x)} = \begin{cases} x & |x| > \lambda \\ 0 & |x| \leq \lambda \end{cases} \tag{2.2}$$

The soft thresholding technique sets zero for all coefficients below the specified threshold value, λ and reduces the magnitude of remaining coefficients by the weighted difference between the transformed coefficients, x and λ, defined as [24]:

$$T_{soft(x)} = \begin{cases} sign(x)(|x| - \lambda) & |x| \geq \lambda \\ 0 & |x| < \lambda \end{cases} \tag{2.3}$$

where

$$sign(x) = \begin{cases} -1 & if\ x < 0 \\ 0 & if\ x = 0 \\ 1 & if\ x > 0 \end{cases}$$

There also exists another thresholding method in the literature, which has been used rarely. It is named semi-soft thresholding, which comprises the two general ones discussed here. Two thresholds value of λ_1 and λ_2 are predefined ($\lambda_1 < \lambda_2$). Semi-soft thresholding sets zero for all coefficients below the threshold λ_1 and retain the magnitude of remaining coefficients that are greater than threshold λ_2, and a weighted average of λ_1 and λ_2 is assigned to the rest coefficients that fall between λ_1 and λ_2, defined in [25, 12]:

$$T_{semisoft\,(x)} = \begin{cases} 0 & |x| \leq \lambda_1 \\ sign(x)\frac{\lambda_2(|x|-\lambda_1)}{\lambda_2-\lambda_1} & |x| \leq \lambda_1 \\ x & |x| > \lambda_2 \end{cases} \tag{2.4}$$

The hard thresholding technique is selected for this project, not only because it can provide a more visual satisfaction denoised result, but also because it can give a better performance resulting in enhanced smoothness [21]. In addition, it can provide an improved numerical value of SNR. SNR is an important parameter to show the effectiveness of the denoise technique. In the literature, SNR is the most frequently used criterion to evaluate the denoised result. Usually, the higher the SNR value, the better the denoised result. On the other hand, the soft thresholding technique generally may introduce more error than the hard thresholding technique [9]. Furthermore, the soft thresholding is believed ineffective denoising in the approximation parts of the signal [26].

2.2.3 Wavelet Selection for Denoising

The selection of the mother wavelet is essential for the purpose of denoising, as it determines the optimal performance of the analyzed signals. Wavelets available in the wavelet family include Gauss wavelet, Haar wavelet, Daubechies wavelets, Bi-othogonal, Coiflets, and Symlets.etc. The proper choice of the mother wavelet could ensure a better approximation. Therefore, it guarantees all the important frequencies are retained in the denoised signal through capturing all the important transient spike values of the original signal [21]. In this project, the Daubechies wavelet is selected for the denoising purpose since it has many successfully utilizations, such as the wavelet-based speech enhancement/denoising [22], e.g., it has optimum denoising performance to the ECG type of signal [35] and to the baseband signals in band-limited channels [24]. Before Daubechies wavelet had been discovered, the Haar, Shannon, and Linear Splines were the ones often used for denoising purpose; however, each of them has major drawbacks. The Haar wavelet is a discontinuous wavelet in wavelet family. Smoothness is an important

property of a wavelet. In continuous wavelets, the Daubechies has better smoothness comparing to others [23], therefore, a better denoised result is ensured.

2.2.4 Denoising Implementation Using Wavelet Toolbox

In Wavelet Toolbox, the threshold value can be automatically determined based on the features of the signal and their statistical properties of the DWT coefficients [24]. Therefore, we do not have to seek algorithms or methods used to determine the best fit threshold value for thresholding the wavelet coefficients. Methods available for classifying the predefined threshold values have been studied extensively; and the efficiency of the thresholding process is always threshold value dependent. Some popular threshold definitions existing in the literature for one-dimensional signals are: Universal Threshold, Wavelet Packet Threshold, Level Dependent Threshold, and Node Dependent Threshold [22].

According to the Wavelet Toolbox uses' guide [10]; the following steps are used to accomplish the whole wavelet denoising process:

1. Start the 1-D wavelet analysis tool from the MatLab command window.

2. Load the signal to be analyzed from the file menu.

3. Perform the three level decomposition process using db3. s, denotes the acceleration signal, $a3$ represents approximations at level 3, and $b1$, $b2$ and $b3$ represent the details at level 1, level 2 and level 3, respectively, as the user interface shown in Figure 2.8:

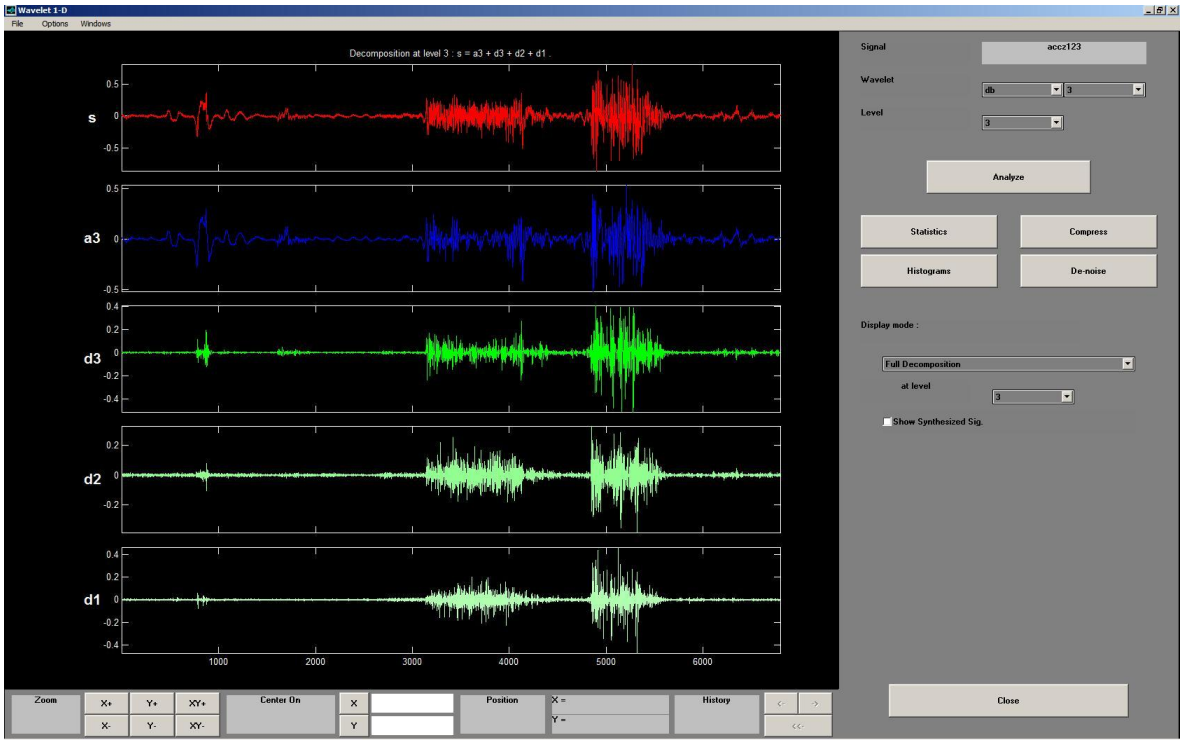

Figure 2.8: Three level decomposition window under Wavelet Toolbox

4. Analyze the signal, by clicking the denoise button on the right hand side of the window, as the close up window is shown in Figure 2.9:

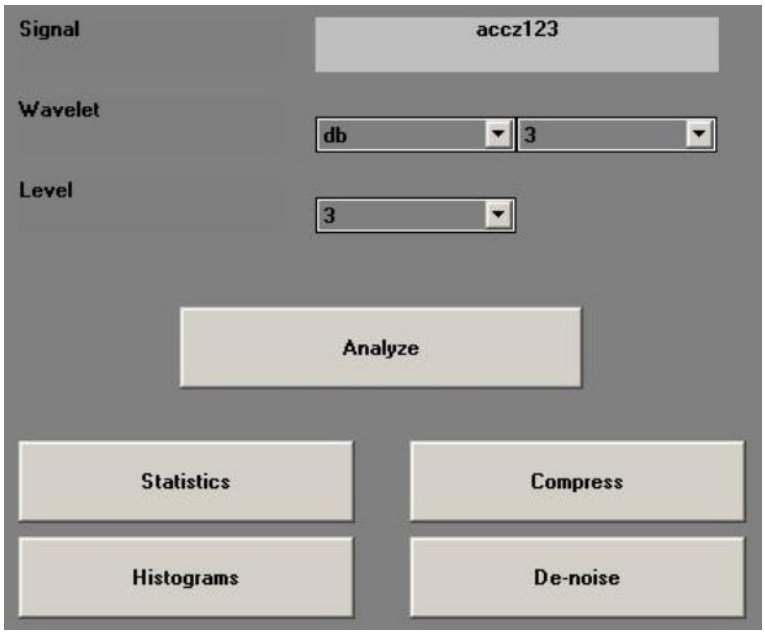

Figure 2.9: The close up window of the three level decomposition under Wavelet Toolbox

5. In this de-noised environment, the un-scaled white noise is selected as the noise structure. The window of the denoising environment is shown in Figure 2.10:

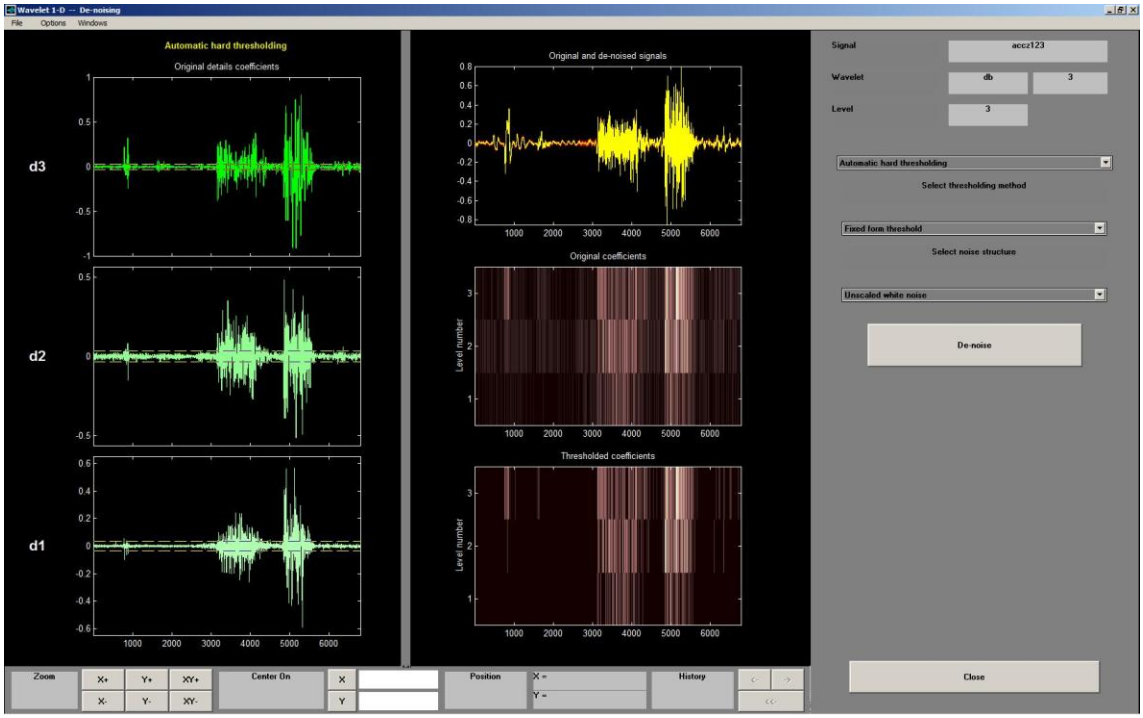

Figure 2.10: Automatic hard thresholding environment

6. Save the de-noised signal by updating the synthesized signal.

2.3 Events Identification Using Clustering Based Algorithm

The collected acceleration data include seven different transient events. Therefore, the clustering based algorithm is developed to classify the acceleration data into seven clusters. One aspect different from other's work, making this new clustering algorithm unique is that the number of clusters is predefined. We need to develop a new and effective clustering algorithm for the acceleration data because many existing clustering algorithms are not applicable for the purpose of events identification in this work [8]. Our goal is to identify the intra-cluster similarity and

inter-cluster dissimilarity within each and between the neighbouring clusters. The spikes variation of the accelerations data is used as the similarity and the dissimilarity measures, and subsequently used to uncover the seven different patterns. The acceleration data classified in the same cluster displays their similarity; and the spikes between the neighbouring sub-clusters shows their maximum dissimilarity.

The clustering process is a thresholding process; therefore, the event clustering begins with the thresholds determination. The threshold value defined for each event's identification depends on the abrupt variation on the distance measure, which is the amplitude or the duration of the acceleration spikes within each section of interest. The selection of the optimum threshold value depends on the typical spikes pattern or feature within the section of interest.

The clustering algorithms developed for the event identification are different for the three-event and four-event sections, as they are signal patterns dependent. In the three-event section, the acceleration pattern for each event is significantly different; therefore, the clustering idea of grouping neighbouring acceleration spikes of similar magnitudes to the same section is used. Theoretically, the ground vehicles should experience higher magnitudes of accelerations during the event segment, and has relatively lower magnitudes of accelerations during the transition section. Therefore, there is a relative spike magnitude change when there is any transaction going on. Most importantly, for each section's identification, those different acceleration patterns between the event and the transition will aid the optimum threshold values selection. However, in the four events section, the acceleration spikes are spread out over the entire section, i.e., there is no unique acceleration pattern for each of the events that can be identified visually. Therefore, a different event identification strategy is employed. The idea of grouping neighbouring spike of similar densities to the same section is used to cluster each of the events. Theoretically, the

ground vehicles should experience high acceleration spike densities during the event section, and has relatively lower acceleration spike densities in the transition section. Therefore, there is a relative acceleration spike density change between a pair of transactions.

The detail clustering procedure starts with the three events section. The high peak values of the acceleration spikes are extracted as P_i, and their corresponding time instances are recorded as T_i. The clustering criterion is to compare the magnitude of the pre-defined threshold value to the magnitudes of P_i in the clustering section. More specifically, the acceleration peaks, P_i evaluated at the moment are assigned to the cluster, which is believed most similar based on a relatively large difference between the magnitude of P_i and the pre-defined threshold. Since the events identification process is a thresholding process, the successful selection of threshold value is essential for each event's identification. First of all, the relationship used to define the threshold value for the events' start time identification is written as:

$$\lambda_S = C \cdot max(S_e),\ e = 1 \dots E_l \tag{2.5}$$

where E_l is the total number of the acceleration spikes of the previous identified event section, S_e. C is a constant determined using the spike patterns of the evaluating section. The evaluation criteria used to find the event start time is to compare the magnitudes of P_i with λ_S. The time instance at which the magnitude of P_i occurs with a larger magnitude than λ_S is the start time of the current evaluating event. Similarly, the start time instances for each of the three events can be found. For example, for the 2nd event identification, which is ¾'' Chatter Bumps as shown in Figure 2.1, the threshold value λ_{2S} is used to identify the 2nd event's start time, it is defined as:

$$\lambda_{2S} = c \cdot max(S_{e1}),\ e1 = 1 \dots E_{1l} \tag{2.6}$$

Where S_{e1} stores the extracted high spikes of the 1st event acceleration data. E_{1l}, is the last spike index in the first event section, and c is a predetermined constant based on the spike profile. The threshold criterion is set for comparing P_{t1}, which consists of the extracted high spikes in the transition section between 1st event, which is 4'' Deep Single Chunck Hole and the 2nd event, to λ_{2S}. The 2nd event's start time instance is found when S_{t1} experiencing relatively large magnitude changes with respective to λ_{2S}.

The relationship used to define the threshold value for the events' start time identification is written as:

$$\lambda_e = D \cdot max(S_t),\ t = 1 \dots T_n \tag{2.7}$$

where T_n is the total number of the acceleration spikes of the previous identified transaction section, S_t. D is the constant determined based on the spikes' characteristics or patterns. The evaluation criteria used to find the event end time instance is to compare the magnitudes of P_i in the current evaluating event section with the pre-determined threshold value, λ_e. The time instance at which P_i has a lower magnitude than $\lambda_e$that occurs for a certain period is the event end time. The same procedure is repeated until all the end time instances of the three events are found. For instance, the threshold value, λ_{2e} used to identify the 2nd event's end time is defined as:

$$\lambda_{2e} = d \cdot max(S_{t1}),\ i = 1 \dots T_{1n} \tag{2.8}$$

where T_{1n} is the index of nth spike extracted from the transition section between the 1st and the 2nd event. d is another predetermined constant. The threshold criterion is to compare P_2, which contains the extracted high spikes in the 2nd event section, to λ_{2e}. The 2nd event's end time

instance is found when S_{2e} experiencing relatively large magnitude changes with respective to λ_{2e}. The start and end times for the 1st and 3rd event can be found similarly.

In the four-event section, the spike magnitude variations are not as significant as the ones from the three-event series, we elect to separate the events based on spikes densities. This can be interpreted as frequency clustering. Similar to the three events section, the same procedure is used to find the high peak values, and the time instances corresponding to those high peaks are recorded as well; they are denoted as P_i and T_i. In addition, the time gap between the adjacent high spikes is defined as T_d, and it is calculated using the Euclidean distance:

$$T_d = T_i - T_j \tag{2.9}$$

where T_i and T_j are the recorded time instances of neighbouring spikes of P_i and P_j. In addition, observation of the acceleration patterns in the four events section aided by the information on the pre-estimated theoretical events durations, we found there are seven significant low peaks spread out regularly in the four events section, as the graph demonstrated in Figure 2.11:

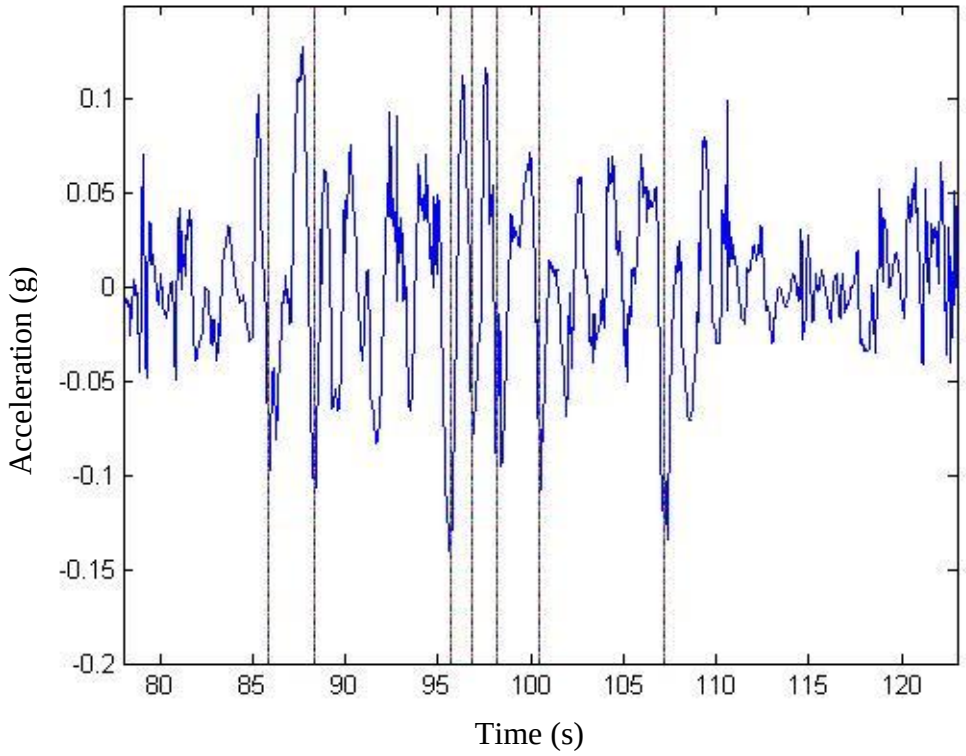

Figure 2.11: extracted seven significant spikes in the first lap four events section using X direction data

Referring to Figure 2.11, those seven significant low peaks, shown as seven vertical lines, are used as the significant characters (features) to cluster. There are three predefined threshold values, they are T_{min}, T_{max} and T_{den}, defined as the minimum searching time, the maximum searching time, and the density of the time gaps. The determinations of T_{min}, and T_{max} are based on the estimated durations for each of the events. The selections of the three optimal threshold values for different sections have to be adjusted by the method of trial and error based on the signal patterns. First of all, the event section or the transition section, in which the significantly low spikes are located, needs to be theoretically identified. Then, the spike can be extracted from the seven significant low spikes to evaluate the corresponding section. Thereafter, based on the extracted significant spike, the time segment to be evaluated can be found. A sample summary of

the sequence of the significant low spikes and the optimal threshold values determined for the four events identification are shown in Table 2.2:

Table 2.2: Summary of the sequence of the significant low spikes and the optimum threshold values used for the four events identification using Z direction first lap counter-clockwise data

significant low spike number	Event section	T_{den}	T_{min}	T_{max}
1	Start of Event4	0.025	0.5	2
2	End of Event4	0.025	0.3	0.8
2	Start of Event5	0.025	0.3	0.8
4	End of Event5	0.025	0.5	2.5
5	Start of Event6	0.025	0.5	3
6	End of Event6	0.025	0.3	2
7	Start of Event7	0.025	0.5	2
7	End of Event7	0.025	0.5	3

According to Table 2.2, the threshold values of T_{den} are the same for each event section, as the spectral contents extracted using peak-to-peak gaps is efficient. The two spikes densities evaluated using three neighbouring spikes are defined as:

$$T_{d(i)} = T_{i+1} - T_i \tag{2.10}$$

$$T_{d(i-1)} = T_i - T_{i-1} \tag{2.11}$$

The threshold criterion is to compare $T_{d(i)}$ and $T_{d(i-1)}$to T_{den}, respectively. If the condition of any spike density has a value greater than the threshold value of T_{den}, then we further compare the searching time with T_{min}, i.e. if $T_d < T_{den}$, the spike being evaluated belongs to the current cluster, otherwise, it belongs to the next event, while the searching time is within T_{min} and T_{max}. In another word, experiencing the acceleration density change as well as the searching time is long enough, the vehicle is undergoing transaction, either from one event to the transition section or from the transition to another event. If the above clustering criterion is not satisfied, we further

compare the searching time with T_{max} to determine the end time of each section. If the searching time is larger than T_{max}, it already goes beyond the section of interest. We record the time instance at T_{i-1} as point of interest. The same procedure is repeated to identify each of the four events' boundaries.

The clustering algorithms that are designed for the events identifications are completed using the computer simulations software of MatLab programs.

2.4 Fourier Analysis

One of the main advantages of using Fourier series analysis is that the frequency components of the acceleration signal can be identified easily, even though there is no information on the time instants at which of the important frequencies take place [28]. In this work, the proposed Fourier based algorithm is a frequency based analysis, and it is mainly used for the refinement of the segmentations of the seven clustered events. As a result, multiple frequency components of the acceleration data can be utilized. The edge refinement process is especially valuable for the four event section. Therefore, to identify the frequency bandwidths for each event is essential, which will be further used for the events segmentation refinement. In addition, the interpolation model or extrapolation model is employed as the basic instrument for the refinement process. Correspondingly, there are two parts in the Fourier refinement process: they are the bandwidth estimation for each of the events, and the event edges refinements using the information about the components frequency difference.

2.4.1 Bandwidth Estimation

The acceleration data is recognized as a band limited signal; it can be characterized by the time bandwidth parameter, τ in Equation (2.12). The determination of τ values is a key step for the whole refinement process. Ideally, based on the sampling theory, τ has a value less than 1, which is to guarantee the convergence of extrapolation result [28]. There will be a variety of significant τ values, i.e., $\tau < 1$ to reflect the character of each portion of the signal; a greater than one value means the signal is under-sampled. In addition, τ value is needed for computing the filter coefficient a_k that appears in the second step of refinement process. τ is the characteristic value for distinguishing a signal with different bandwidths, and it is written as:

$$\tau = \sigma * T \tag{2.12}$$

In the acceleration signal, denoted as $f(t)$, the sampling interval T, specified as 0.005 seconds. where σ, is the bandwidth of $f(t)$. If $w > \sigma$, the signal has transform of £ $\{ f(t)\}$ = 0. The bandwidth σ is estimated by observing a data segment of interest from the acceleration signal. The estimated σ value does not have to be as accurate as in theory. Therefore, we call this estimated bandwidth the nominal bandwidth, denoted as $\hat{\sigma}$. In the acceleration data, the similar peaks are used to estimate the frequency bandwidth. In addition, if it is extremely difficult to estimate the bandwidth through clustering similar peaks, a nominal frequency bandwidth with a number close to but less than 1/(T) will be used instead. This will lead to the nominal τ value close to one, however, it does reflect the character of the signal. The estimated bandwidth $\hat{\sigma}$ is then used to refine the boundary between events or so-called edge refinement. The relationship used to calculate $\hat{\sigma}$ is estimated from:

$$\hat{\sigma} = \frac{\hat{\tau}}{T_d} \tag{2.13}$$

where $\hat{\tau}$ is the estimated time-bandwidth product, shown in Equation (2.13). T_d is the time duration of the similar peaks within an interested time interval. For instance, if we assume T_2 is the time instance of the end of one event to be determined, and T_3 is any time instance that belongs to the following neighbouring section. Then T_2 can be known once the nominal bandwidth $\hat{\sigma}$ is available to formulate the filter over the time section of (T_1, T_2), according to the fact that the acceleration signal has different bandwidths between different sections, e.g. (T_1, T_2) and (T_2, T_3). In addition, the determination of T_2 is based on the variation of the error of extrapolation. Therefore, to observe when there is a sudden change in the extrapolation error is important, which leads to the second step of the refinement process.

2.4.2 Boundary Refinement

The equation governing the one step extrapolation model is given in terms of a convolution:

$$f(t) = \sum_{k=1}^{N} a_k * f(t - kT) \tag{2.14}$$

where $f(t)$ is the signal value to be extrapolated at time t, $f(t - kT)$ are the signal samples (acceleration data), and a_k is the filter coefficient. Firstly, the constant a_k needs to be found, and it can be determined by minimizing the error of the extrapolation model, the error equation is give as:

$$e = \left| f(t) - \sum_{k=1}^{N} a_k * f(t - kT) \right|^2 \tag{2.15}$$

The coefficients matrix of the filter, a_k can be determined from the error estimation of the interpolation in Equation (2.15) [27], In the derivation, we used the Cauchy-Schwarz inequality, Parseval's identity [27], and Euler's formula. The detailed derivation procedures are shown respectively with each of the properties integrated [9]:

$$e = |f(t) - \textstyle\sum_{k=1}^{N} a_k * f(t - kT)|^2 \tag{2.16}$$

$$\leq \frac{1}{4\pi} \int_{-\sigma\pi}^{\sigma\pi} \left| F(w) e^{iwt} \right|^2 dw \int_{-\sigma\pi}^{\sigma\pi} \left| 1 - \sum_{k=1}^{N} a_k e^{-iwkT} \right|^2 dw$$

$$= \frac{1}{4\pi} \int_{-\sigma\pi}^{\sigma\pi} |F(w)|^2 \, dw \int_{-\tau}^{\tau} \left| 1 - \sum_{k=1}^{N} a_k e^{-iwk} \right|^2 dw$$

$$= \frac{1}{2\pi} \|f\|^2 \int_{-\sigma}^{\sigma} \left| 1 - \sum_{k=1}^{N} a_k e^{iwkT} \right|^2 dw$$

To minimize the integral $\int_{-\sigma}^{\sigma} \left| 1 - \sum_{k=1}^{N} a_k e^{iwkT} \right|^2 dw$ is equivalent to minimize the interpolation error e, as the value of $\frac{1}{2\pi}\|f\|^2$ in front of this integral is a constant. We set $d_n = \int_{-\sigma}^{\sigma} \left| 1 - \sum_{k=1}^{N} a_k e^{iwkT} \right|^2 dw$. To minimize d_n, we apply the formula of integration by parts twice and substitute the time bandwidth product Equation (2.12) into the derivation. The final derived relationship to estimate a_k is written as:

$$-\frac{2}{\pi T j} \sin(j\sigma\tau) + \frac{2}{\pi T (j-k)} \sum_{k=1}^{N} \mathrm{a_k} \, (\sin(j-k)\pi\tau) = 0, \quad j = 1,2, \ldots \ldots N \tag{2.17}$$

The filter coefficients in Equation (2.17) satisfy the following system:

$$\begin{bmatrix} 1 & \frac{2}{(-1)\pi\tau}\sin(-1)\tau & \dots & \frac{2}{(1-N)\pi\tau}\sin(1-N)\tau \\ \frac{2}{\pi\tau}\sin\tau & 1 & \dots & \frac{2}{(2-N)\pi\tau}\sin(2-N)\tau \\ \dots & \dots & \dots & \dots \\ \frac{2}{(N-1)\pi\tau}\sin(N-1)\tau & \frac{2}{(N-2)\pi\tau}\sin(N-2)\tau & \dots & 1 \end{bmatrix} \begin{bmatrix} a_1 \\ a_2 \\ \vdots \\ a_N \end{bmatrix} = \begin{bmatrix} \frac{2}{\pi\sigma}\sin\tau \\ \frac{2}{2\pi\sigma}\sin(2\tau) \\ \vdots \\ \frac{2}{N\pi\sigma}\sin N\tau \end{bmatrix} \quad (2.18)$$

To express the filter coefficients, a_k in terms of the *sinc* function, which is defined as $\frac{\sin(Nx)}{Nx}$, we have:

$$\begin{bmatrix} sinc(0) & sinc(\tau) & \dots & sinc(N-1)\tau \\ sinc(\tau) & sinc(0) & \dots & sinc(N-2)\tau \\ & \dots & & \dots \\ sinc(N-1)\tau & sinc(N-2)\tau & \dots & sinc(0) \end{bmatrix} \begin{bmatrix} a_1 \\ a_2 \\ \vdots \\ a_N \end{bmatrix} = \begin{bmatrix} sinc\tau \\ sinc(2\tau) \\ \vdots \\ sinc(N\tau) \end{bmatrix} \quad (2.19)$$

The filter length N can be chosen based on the size of τ. Normally, the larger the τ value the greater the N. However, practically *N* is usually less than 20. The variation of prediction error *e* in Equation (2.16) implies the change in bandwidth, τ. The variation in bandwidth, τ in turns indicates the boundary of the event.

The above coefficients matrix system equation in Equation (2.19) has the general form of:

$$Ax = b \quad (2.20)$$

where A is the coefficients matrix of the filter, x is the column vector of filter coefficient a_k. b is the column vector of the $sinc$ functions. Then the filter coefficient a_k can be determined thereafter, shown as:

$$x = A^{-1} \cdot b \quad (2.21)$$

In addition, the multi-step extrapolation model is given similarly as the one-step extrapolation model:

$$f(t+nT) = \sum_{k=1}^{N} b_k * f(t-kT)\,,\ k=1, 2 \ldots \mathrm{N} \tag{2.22}$$

where $f(t+nT)$ is the value to be estimated from the acceleration signal at time $(t+nT)$, $f(t-kT)$ are the samples of the acceleration signal. Similarly, b_k is the filter coefficient to be estimated.

The filter coefficients matrix for the multi-step extrapolation model is derived using the same procedure as the one-step extrapolation model. The system coefficients matrix A derived for n-step extrapolation model is the same as the one-step extrapolation, therefore, it is independent of the number of steps of the extrapolation; it is a special merit of the extrapolation model. However, b value is dependent on the steps of the extrapolation, b derived of n-step extrapolation model is:

$$\begin{bmatrix} sinc(1+n)\tau \\ \vdots \\ sinc(N+n)\tau \end{bmatrix} \tag{2.23}$$

Correspondingly, the filter coefficient b_k of the multi-step extrapolation can be determined via the same procedure detailed for the filter coefficient a_k, a column vector of x can be determined from the system Equation (2.21).

The proposed extrapolation model for events refinement is programmed in MatLab.

3. Chapter 3

Mission Profile, Full-Period PSD Profile, Partial-Period Driven Profile Generation of Accelerated Durability Test

The mission profiles of accelerated durability test can be generated using the correlated acceleration data with events periods as discussed in Chapter 2. The accelerated durability test with the desired testing period is defined as the full-period accelerated durability test. The corresponding mission profiles and PSD profiles are called full-period accelerated durability test mission profiles and PSD profiles, respectively. However, the full-period PSD data cannot be practically applied in the lab due to required tuning of each actuator. Therefore, the generation of the shorter acceleration data which contains the major features of the full-period test PSD data is required, and such shorter acceleration data will be repeated to generate the same fatigue damaging content. The shorter acceleration data, its corresponding PSD and duration are defined as those of the partial-period accelerated durability test. As a result, to implement the generated full-period PSD, partial-period driven profile needs to be further created. The mission profiles, full-period PSD profile, and the partial-period driven profile can be generated using the Mission Profiling, Test Synthesis, and Custom Fourier processes, respectively under the existing commercial software of the nCode ICE-FLOW GlyphWorks [1].

In the Mission Profiling process, the input is the correlated acceleration data with the corresponding events, and the output is the Fatigue Damage Spectrum (FDS), and Shork

Response Spectrum (SRS) of each event. In the Test Synthesis process, the input is the mission profiles, consisting FDS and SRS of all the events with necessary occurrence expected in the field test, the output is the full-period PSD profile. Finally, the partial-period accelerated durability test can be best achieved by using a so called "Custom Fourier" process using the same software of GlyphWorks, of which the input is the full-period PSD data, and the output is the partial-period acceleration data. In this project, the field test duration is 650 hours, the full-period test durations are 24 and 48 hours, and the length of the partial-period test load is 60 seconds. The general procedures of the systematic accelerated durability test conduction process are summarized in Figure 3.1:

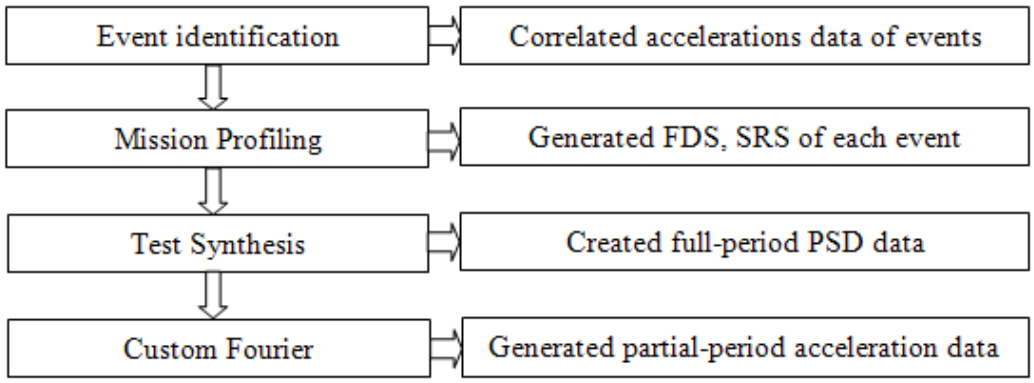

Figure 3.1 General procedure for the accelerated durability test conduction process

Referring to Figure 3.1, the generation of PSD for the full-period accelerated durability test is the essential step to further precede the partial-period accelerated test. The methodologies used to generate the mission profiles of accelerated durability test will be presented in section 3.1. In section of 3.2, the method of generating the full-period accelerated test PSD, e.g. 24 hours will be shown. In addition, the method of comparing the full-period accelerated durability test with the field test is also presented. In section 3.3, the generation of a partial-period accelerated test, e.g. 60 seconds acceleration data will be discussed. In section 3.4, the method of validating the

partial-period accelerated test will be detailed. In section 3.5, parametric analysis of key parameters on the important profiles of partial- period accelerated test is carried out.

3.1 Generation of Accelerated Durability Test Mission Profiles

Important response spectrums introduced in the accelerated durability test includes Power Spectrum Density (PSD), Shock Response Spectrum (SRS), Fatigue Damage Spectrum (FDS), and Extreme Response Spectrum (ERS); they're plotted and defined in the frequency domain. The definition of each spectrum is defined below:

Power Spectrum Density (PSD)-PSD is a measure of the power of a signal over a range of frequencies, and it is a frequency plot in unit g^2/HZ.

Shock Response Spectrum (SRS)-SRS is a specification of the maximum response of a time domain signal over a range of frequencies, it is a frequency plot in unit of gravity acceleration, g.

Extreme Response Spectrum (ERS)-ERS is the specification of the expected maximum response of a random vibratory signal over a range of frequencies; it is a frequency plot in unit of g.

Fatigue Damage Spectrum (FDS)-FDS is a non-dimensional specification of the expected damage accumulated by a component over a range of frequencies.

All the above response spectrums are determined by sweeping the natural frequency of the system while assuming the system experiences resonance at each natural frequency [2]. Therefore, all the response spectrums are expected to represent the most damaging scenario for the testing component at each frequency.

The SRS and FDS for each event need to be determined first, and then the mission profiles of all the events that consist of the sum of all FDS and the maximum envelope of all SRS with the necessary repeats of 330 hours field test can be determined thereafter [1].

3.2 Generation of Full-period Accelerated Durability Test PSD

A synthesized accelerated test PSD can be created from events FDS, SRS. The FDS of the accelerated test and the original data have to be similar, and the envelope of the ERS profile of the synthesized accelerated test has to be identical to or below the SRS of the field test to ensure no unrealistic loads are generated. At the same time, they should still be similar to avoid any change in failure mechanism. The general steps for a synthesized accelerated test PSD generation is summarized in the Figure 3.2 [1]:

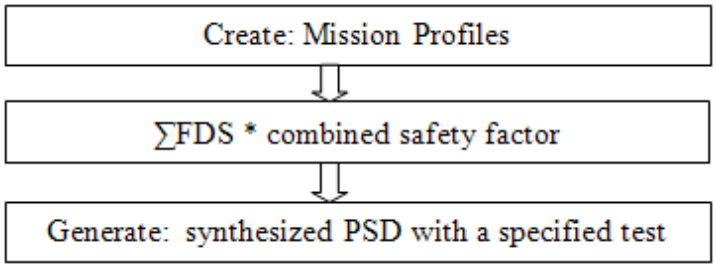

Figure 3.2: Method for generating full-period accelerated durability test PSD profile

Referring to Figure 3.2, the fatigue content contained in the generated PSD will have the same fatigue content of field testing multiply by the combined safety factor, kc. It is important to obtain kc as it account for any part damage and environment damage increase. Other important non-dimensional statistical factors of generating accelerated test consist of safety factor, ks and test factor, kt. They have a relationship shown in Equation (3-1):

$$kc = ks \cdot kt \tag{3.1}$$

In Equation (3-1), ks and kt can be determined from both of GlyphWorks and manual calculations. The relationships used to determine factors of ks and kt are shown respectively in Equations (3-2) and (3-3) [2]:

$$ks = \exp\left(a's\sqrt{\ln\left[(1+V_e^2)(1+V_r{}^2)\right]} - \ln\sqrt{\frac{1+v_e{}^2}{1+V_r^2}}\right) \tag{3.2}$$

$$kt = \exp\left(\frac{a't}{\sqrt{nt}}\sqrt{\ln\left[\left(1+V_r{}^2\right)\right]}\right) \tag{3.3}$$

Where $a's$, is the probability of success, $a't$ is the confidence level. Ve is the variability of environment damage, and V_r is the variability of component damage resistance. Therefore, the combined safety factor, kc will ensure that all the damaging variability are considered. In addition, the relationship used to define PSD at various natural frequencies in terms of FDS, and the relationships used to define the FDS and ERS are shown as [2]:

$$PSD(f_n) = \frac{2(2\pi\cdot f_n)^3}{Q}\left[\frac{k_c\cdot\sum FDS(f_n)\cdot C}{K^b\cdot f_n\cdot T\cdot\Gamma\left(1+\frac{b}{2}\right)}\right]^{\frac{2}{b}} \tag{3.4}$$

$$\Gamma(g) = \int_0^\infty x^{(g-1)}e^{-x}dx \tag{3.5}$$

$$FDS(f_n) = f_n\cdot T\frac{k_c^b}{C}\left[\frac{Q\cdot PSD(f_n)}{2(2\pi f_n)}\right]^{\frac{2}{b}}\cdot\ \Gamma\left(1+\frac{b}{2}\right) \tag{3.6}$$

$$ERS(f_n) = [\pi f_n\cdot Q\ \cdot PSD(f_n)\cdot\ln(f_n\cdot T)]^{\frac{1}{2}} \tag{3.7}$$

Where K is the stress to displacement factor, Q is the dynamic amplification factor, C and b are the Intercept and Slope of S-N curve defined in GlyphWorks [1].

There is an accelerated test period required for each PSD generation [1]. Therefore, the testing period actually determines the magnitude of the generated PSD. The relationship used to specify the magnitude of the PSD and the accelerated test period is defined as:

$$PSD \propto (\frac{1}{T_{test}})^{\frac{2}{b}} \tag{3.8}$$

Equation (3-8) reveals that a higher magnitude of PSD will result from a lower value of the test period used. That is why the accelerated test PSD always has a higher magnitude level than the original field test PSD. In Equation (3-8), there is another parameter affecting the magnitude of the generated accelerated test PSD, denoted as b, which is related to the property of the material. The b values recommended for different materials are shown in the Table 3.1 [2]:

Table 3-1: b values recommended for different materials

Material	Value range
Brittle material	4 or less
Ductile material	4 to 8

As a result, the brittle material will produce a higher magnitude of PSD compare to the ductile material, as the b value used for the brittle material is lower than for the ductile material.

The numerical values of the parameters used to generate 24 hours and 48 hours PSDs were adapted from the report of Generation and Verification of Accelerated Durability Test [2], summarized in Table 3.2 and Table 3.3:

Table 3-2: The numerical values of the parameters for 24 hrs accelerated test PSD generation

Property	Value
K	1
b	6
C	1
Q	10
V_R	8%
n_{test}	1
a'_{test} (corresponding confidence level in percentage)	1.6449 (95%)
Test Factor Distribution	Log-normal
k_t	1.14
k_s	1

Table 3-3: The numerical values of the parameters for 48 hrs accelerated test PSD generation

Property	Value
K	1
b	6
C	1
Q	10
V_r	8%
n_{test}	1
a'_{test} (corresponding confidence level in percentage)	1.6449 (95%)
Test Factor Distribution	Log-normal
k_t	1.14
V_e	22.5%
a'_{safety} (corresponding probability of failure in percentage)	3.09025 (0.1%)
Safety Factor Distribution	Log-normal
k_s	2.03

Both of the 24 hours and 48 hours accelerated test PSDs are generated with respect to the original 330 hours field test PSD in this work.

The full-period accelerated durability test PSD, FDS, and ERS have to be compared with the original field test PSD, FDS and SRS to ensure no unrealistic high load and failure mechanism changes. The flow charts of the general procedures used for validating an accelerated durability test are shown in Figure 3.3:

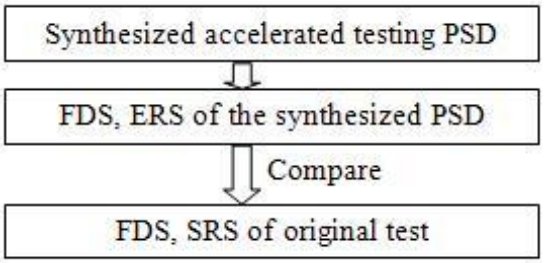

Figure 3.3: Method for validating accelerated durability test

Referring to Figure 3.3, the synthesized full-period accelerated test PSD is generated from the mission profile FDS with the information on the combined safety factor, kc. To validate an accelerated durability test, the comparison between the mission profiles of accelerated test and field test is necessary. Ideally, the FDS of the accelerated test and the original data have to be similar, and the envelope of the ERS profile of the synthesized accelerated test has to be identical to or below the SRS of the field test to ensure no unrealistic loads are generated; at the same time, they should still be similar to avoid any change in failure mechanism [1].

3.3 Generation of Partial-period Test Driven Profile

To practically apply vibration loads on the testing components on MAST, partial-period accelerated durability test needs to be further conducted using the full-period test profiles, as the last step shown in Figure 3.1. In this section, the generation of acceleration time series of the partial-period test using the software of the GlyphWorks is introduced [2]. Referring to Figure

3.1, the generation of the acceleration data for the partial-period test can be further processed based on the generated 24 hours PSD data [2]. The partial-period using 60 seconds acceleration data is chosen, because it can be practically implemented in the lab test, such as the cost to tune each of the actuators is significantly low.

As a result, the 60 seconds acceleration data can be directly applied as the vibration load on MAST, and continually repeated. To ensure the same fatigue damage content observed relates to the field test, the number of repeats is needed and calculated using equation expressed as [2]:

$$Num_{repeats} = \frac{T_{full}}{T_{partial}} \tag{3.9}$$

Where the T_{full} is the full-period of accelerated test used, e.g. 24 hours, 48 hours. $T_{partial}$ is the partial-period, e.g. 60 seconds. As a result, the number of repeats determined for 60 seconds partial test using 24 hours and 48 hours full accelerated test periods are 1440 and 2880. The linear addition of the partial-period test FDS with the number of repeats achieve the field test FDS [2]. The synthesized PSD, ERS and FDS for a partial-period test can be correspondingly determined using the acceleration data [1]. Parameters need to be correctly defined for the effective ERS and FDS generations. The only parameter believed essential for the generation of the two primary indicators of ERS and FDS for the partial-period test, is the slope *b*, which is also called fatigue parameter introduced earlier [1]. Generally, a relative higher value of *b* will accelerate the partial-period test more drastically without obtaining unrealistic stresses [1].

3.4 Validation of Partial-period Test Driven Profile

To ensure that the partial-period test acceleration data capture most dynamic features of the full-period test PSD, validation is needed. The important profiles of the partial-period test are

compared with the original filed test data to validate a partial-period accelerated durability test. Using the validation criteria stated in section 3.2, both of the generated FDS and ERS for the partial-period test periods have to be compared with the field test mission profiles consist of FDS and SRS. To have a validate 60 seconds partial accelerated durability test, the FDS of the partial-period test have to be similar to the original data. Most importantly, the envelope of the ERS profile of the partial-period test has to be below or equivalent to the SRS profile of the field test to ensure no unrealistic loads are generated; at the same time, they should be still similar to avoid any failure mechanism changes occurs [1].

3.5 Parametric Analysis on the Important Profiles

As demonstrated in section 3.1, Test Period, T_{test} and Fatigue Parameter, b are important for the generation of efficient PSDs. Parametric analysis of T_{test} and b on the efficient PSDs generation of the partial-period test will be conducted. Other partial test periods of 3 minutes and 5 minutes are selected in order to study the sensitivity of T_{test} on the effective PSD generation for the partial-period test. To obtain those shorter vibration loads for the lab tests, the generated 24 hours PSD profile will be used. To ensure a valid partial-period test is generated, the frequency contents and the power contents of the partial-period test have to be checked. As a result, the frequency content and the power content of the partial-period test PSD needs to be compared with the full-period test PSD. Most importantly, the maximum power occurrence of the partial-period test has to be similar to the field test to ensure no failure mechanism changes of the testing vehicle. In addition, 1 HZ and 7 HZ are the frequencies of the resonance occurrences of the testing vehicle; therefore, maximum power has to be checked at those two frequencies when various partial test periods used. In addition, the effect of the fatigue parameter, b on the efficient

partial-period test PSDs generation is studied. Different values of b 2, 4, 6, and 8 are used to generate the 60 seconds PSDs respectively.

As stated earlier in section 3.3, the only parameter that is believed to have an effect on the validation process of the partial-period test, which is used for the effective ERS and FDS generation is the slope, also called fatigue parameter, b. In order to check the sensitivity of b used in the partial-period test validation process, same values of parameter b2, 4, 6 and 8 are modified and used respectively for the generation of 60 seconds ERS and FDS. A valid partial-period accelerated durability test requires the ERS below or equivalent to the SRS, and FDS resemble FDS of the field test data. Values of b that violate the validation criteria cannot be used for future work.

4. Chapter 4

Main Results and Discussions

In this chapter, results of events identification, the generated mission profiles, full-period test PSD profiles, partial-period test loading profile, and results of parametric analysis will be presented, respectively, along with discussions. In addition, results of partial-period test with respect to the field test are compared for validation.

4.1 Events Identification

The results of the denoised acceleration data using Wavelet Toolbox, the acceleration data of the identified events and the refined events will be shown respectively in the following subsections.

4.1.1 Wavelet Denoised Acceleration Data

The set of the field test time series used to identify the events and to generate the accelerated vibration driven profiles are accelerations collected from the proving ground field track test at the Pennsylvania Transportation Institute [4]. The collected data of the accelerations in the driving (X) and vertical (Z) directions, shown in Figure 2.3 (a), are denoised through Wavelet Toolbox using db3 and hard thresholding. One sample denoised result of three- and four-event sections, shown in Figure 2.3 (b) with respect to the original acceleration data of the field test are shown in Figure 4.1 and Figure 4.2, the vertical axis is the accelerations in the unit of g, and the horizontal axis is the time in the unit of second.

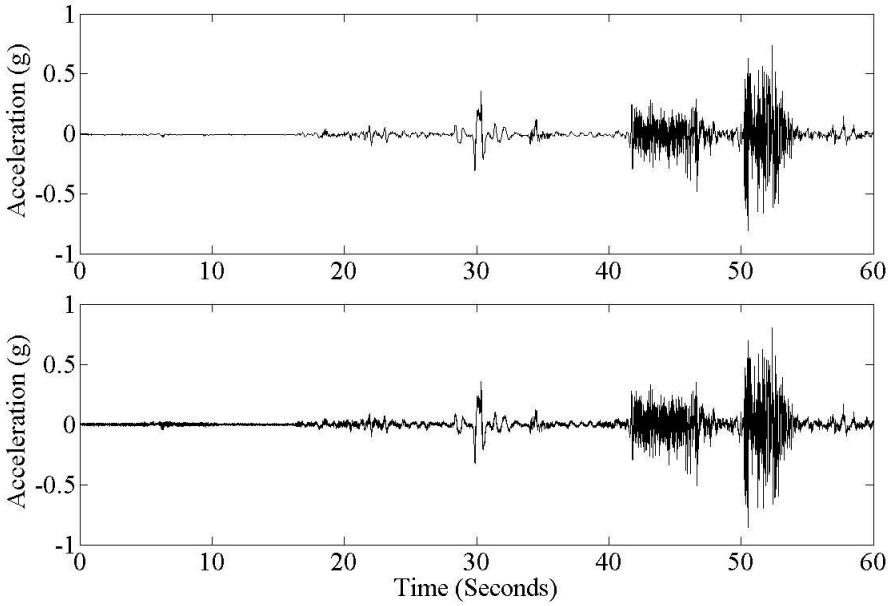

Figure 4.1: The acceleration time series for the three-event section in the Z direction from the 1st set counter-clockwise lap (a) denoised and (b) original

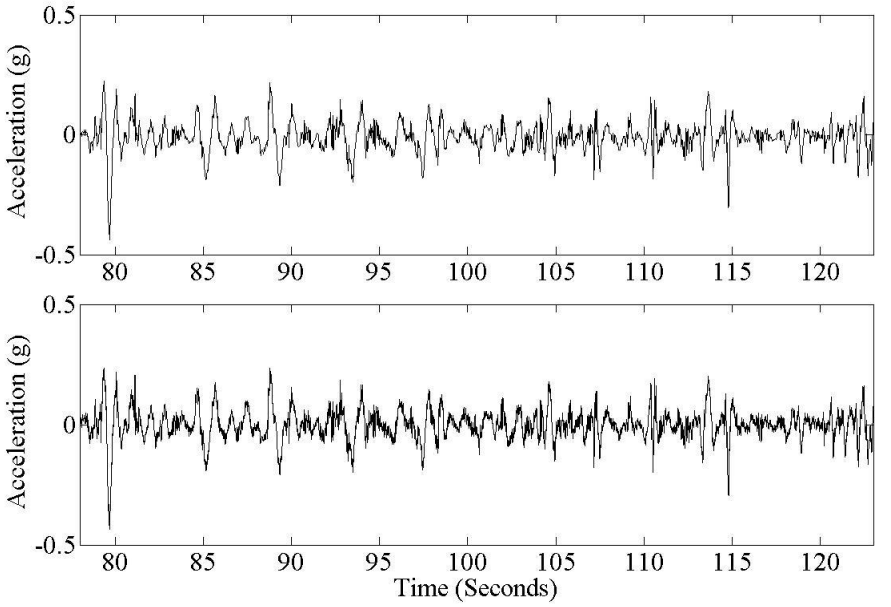

Figure 4.2: The acceleration time series for the three-event section in the Z direction from the 1st set counter-clockwise lap (a) denoised and (b) original

As Figure 4.1 demonstrated, the denoised three-event acceleration data keep the same general trends as the original one, while the original signal has a higher density as compared to the

denoised one. Therefore, the important information which contains the low frequency components is maintained. Similar results have been found from the acceleration data of the four-event section, as shown in Figure 4.2, as well as from the acceleration data in the X direction.

4.1.2 Events Identification and Refinement

The new designed clustering based algorithm and Fourier frequency based method are applied on the wavelet denoised acceleration data in the X, and Z translational directions, as shown in Figure 4.3, to cluster and to refine the events segments respectively. The results of events identification, which are the acceleration data with the correlated field test events, will be shown. The start time and the end time of each event found during the three counter-clockwise laps and three clockwise laps using the above two methods are shown respectively in sections 4.1.2.1 and 4.1.2.2.

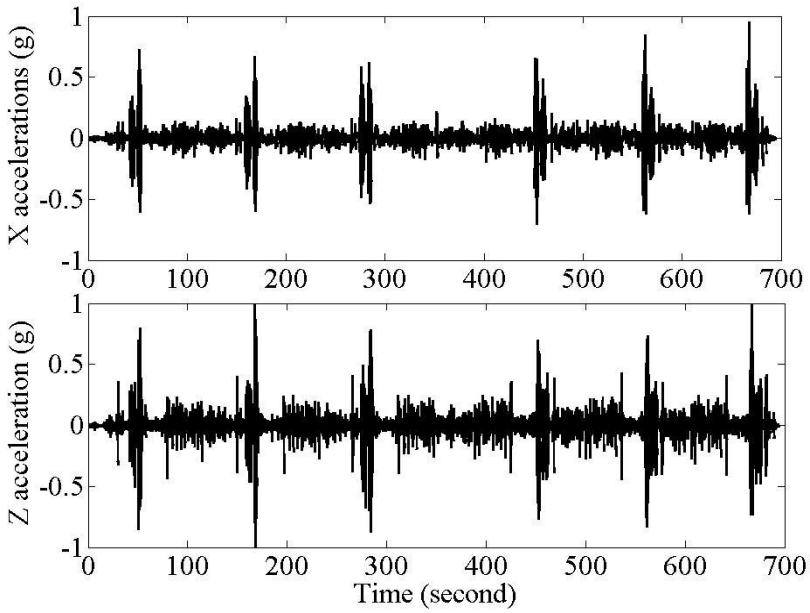

Figure 4.3: Accelerations in X and Z directions for 6 laps from field tests

4.1.2.1 Events Identification Using Clustering Method

The start and the end time instances of three and four events, as shown in Table 2-1, are successfully found by using the new clustering algorithm. The seven events in sequence are 4" Single Chuck Hole, 3/4" Chatter Bumps, 1" Random Chuck Holes, Railway Crossing, Staggered Bumps, Frame Twist, High Crown Intersection. The first, second, and third counter-clockwise laps start at the time instance of 26 second, 170 second, and 263 second respectively. The first, second, and third clockwise laps start at the time instance of 393 second, 487 second, and 606 second respectively. The identified results of three counter-clockwise and three clockwise laps using Z and X directions data are summarized from Table 4.1 to Table 4.4:

Table 4.1: Identified three events of counter-clockwise laps using the acceleration data in the Z and X directions

Transactions	1st Lap (s)		2nd Lap (s)		3rd Lap (s)	
	Z direction	X direction	Z direction	X direction	Z direction	X direction
Start of Event1	28.26	29.955	148.11	149.645	264.17	265.715
End of Event 1	34.82	35.215	153.82	154.34	270.33	272.225
Start of Event2	40.53	41.695	158.43	158.455	274.29	274.425
End of Event 2	46.15	47.895	164.74	164.82	280.44	281.955
Start of Event3	50.49	50.26	167.05	167.06	282.61	282.865
End of Event 3	54.71	55.705	172.05	174.305	288.03	289.415

Table 4.2: Identified four events of counter-clockwise laps using the acceleration data in Z and X directions data

Transactions	1st Lap (s)		2nd Lap (s)		3rd Lap (s)	
	Z direction	X direction	Z direction	X direction	Z direction	X direction
Start of Event 4	79.26	78.79	195.74	198.6	315.89	315.06
End of Event 4	84.37	84.66	201.46	203.85	321.16	320.05
End of Event 5	94.91	95.06	212.22	214.49	332.62	328.75
Start of Event 6	99.1	99.14	216.26	219.62	336.29	333.06
End of Event 6	105.49	105.33	223.02	224.76	342.65	339.54
Start of Event 7	109.85	110.86	227.44	229.69	347.44	343.63
End of Event 7	115.61	117.36	233.07	234.74	352.31	348.74

Table 4.3: Identified three events of clockwise laps using the acceleration data in the Z and X directions

Transactions	1st Lap (s)		2nd Lap (s)		3rd Lap (s)	
	Z direction	X direction	Z direction	X direction	Z direction	X direction
Start of Event1	394.33	392.42	498.11	495.22	607.18	602.71
End of Event 1	401.31	397.74	506.08	501.67	615.58	610.79
Start of Event2	402.13	402.45	507.13	507.25	616.52	617.57
End of Event 2	409.88	409.26	514.98	512.49	623.97	623.34
Start of Event3	410.15	410.37	515.24	515.29	624.41	624.73
End of Event 3	416.58	414.84	520.82	518.62	630.37	631.53

Table 4.4: Identified four events of clockwise laps using the acceleration data in the Z and X directions

Transactions	1st Lap (s)		2nd Lap (s)		3rd Lap (s)	
	Z direction	X direction	Z direction	X direction	Z direction	X direction
Start of Event 4	437.73	436.63	545.49	545.88	651.29	650.46
End of Event 4	441.16	441.38	551.22	551.17	656.82	656.01
End of Event 5	452.54	452.07	562.13	561.86	667.46	667.13
Start of Event 6	456.54	456.26	566.17	566.25	671.13	671.15
End of Event 6	462.57	462.9	572.89	573.21	677.93	677.77
Start of Event 7	467.77	467.45	577.36	577.51	682.15	682.26
End of Event 7	473.31	472.89	583.13	583.09	687.25	687.93

According to the results of the identified events using new clustering algorithm from Table 4.1 to Table 4.4, the start and the end time instances of the events using X and Z directions are quite

close, indicating the success of the clustering algorithm. To improve the accuracy of the identified events, further refinement process using Fourier analysis is needed based on the clustered results.

4.1.2.2 Events Refinement Using Fourier Analysis

The start and the end time instances of the events are refined using Fourier analysis on the initial clustered results that are summarized in section 4.1.2.1. The refined start and the end time instances of each event using the acceleration data in the X and Z directions from three counter-clockwise and three clockwise laps are summarized from Table 4.5 to Table 4.8:

Table 4.5: Refined start and end time instances for the three events of counter-clockwise laps using the acceleration data in the Z and X directions

	1st Lap (s)		2nd Lap (s)		3rd Lap (s)	
Transactions	Z direction	X direction	Z direction	X direction	Z direction	X direction
Start of Event1	28.76	29.255	148.26	149.255	264.26	265.255
End of Event 1	34.76	35.255	153.42	154.255	270.26	272.255
Start of Event2	40.76	41.255	158.26	158.26	274.26	274.26
End of Event 2	46.26	47.255	164.75	164.26	280.76	281.255
Start of Event3	50.26	49.755	166.76	166.755	282.25	282.255
End of Event 3	54.76	55.255	172.26	174.255	288.26	289.26

Table 4.6: Refined start and end time instances for the four events of clockwise laps using the acceleration data in the Z and X directions

	1st Lap (s)		2nd Lap (s)		3rd Lap (s)	
Transactions	Z direction	X direction	Z direction	X direction	Z direction	X direction
Start of Event 4	79.26	78.55	196.06	198.26	315.76	315.26
End of Event 4	84.26	84.26	201.26	203.26	321.26	320.76
Start of Event 5	84.26	84.26	201.26	203.26	321.26	320.76
End of Event 5	94.76	94.76	212.26	213.76	331.76	328.76
Start of Event 6	98.75	98.76	216.26	218.76	335.76	333.26
End of Event 6	105.26	105.26	223.26	224.26	342.26	339.76
Start of Event 7	109.76	110.26	227.26	228.76	347.26	343.76
End of Event 7	115.26	116.26	233.26	234.26	352.76	348.96

Table 4.7: Refined start and end time instances for the three events of clockwise laps using the acceleration data in the Z and X directions

Transactions	1st Lap (s)		2nd Lap (s)		3rd Lap (s)	
	Z direction	X direction	Z direction	X direction	Z direction	X direction
Start of Event1	393.26	392.26	496.76	495.86	606.26	603.26
End of Event 1	398.76	397.76	503.76	501.26	613.76	609.76
Start of Event2	402.26	402.76	507.26	507.26	616.76	617.26
End of Event 2	409.76	408.76	514.75	512.26	623.76	623.26
Start of Event3	410.26	410.26	515.26	514.75	624.76	624.86
End of Event 3	414.76	414.76	518.71	518.18	629.76	629.76

Table 4.8: Refined start and end time instances for the four events of clockwise laps using the acceleration data in the Z and X directions

Transactions	1st Lap (s)		2nd Lap (s)		3rd Lap (s)	
	Z direction	X direction	Z direction	X direction	Z direction	X direction
Start of Event 4	436.76	436.26	545.96	546.26	650.96	650.96
End of Event 4	441.26	441.26	551.26	551.26	656.26	655.76
Start of Event 5	441.26	441.26	551.26	551.26	656.26	655.76
End of Event 5	452.26	451.76	561.76	561.76	667.26	667.26
Start of Event 6	456.26	456.26	566.26	566.26	671.26	670.76
End of Event 6	462.56	462.76	572.76	573.26	677.76	677.26
Start of Event 7	467.26	467.26	577.26	577.26	681.76	682.26
End of Event 7	473.26	472.76	583.26	582.76	686.96	687.26

As shown from Table 4.5 to Table 4.8, the refined start and the end time instances of seven events using the acceleration data in the Z and X directions are closer with respect to the clustering results, shown from Table 4.1 to Table 4.4. The sample simulation results of the refined three and four events are plotted accordingly from Figure 4.4 to Figure 4.7. For the following figures, the vertical axis is the acceleration in the unit of g, and the horizontal axis is the time in the unit of second.

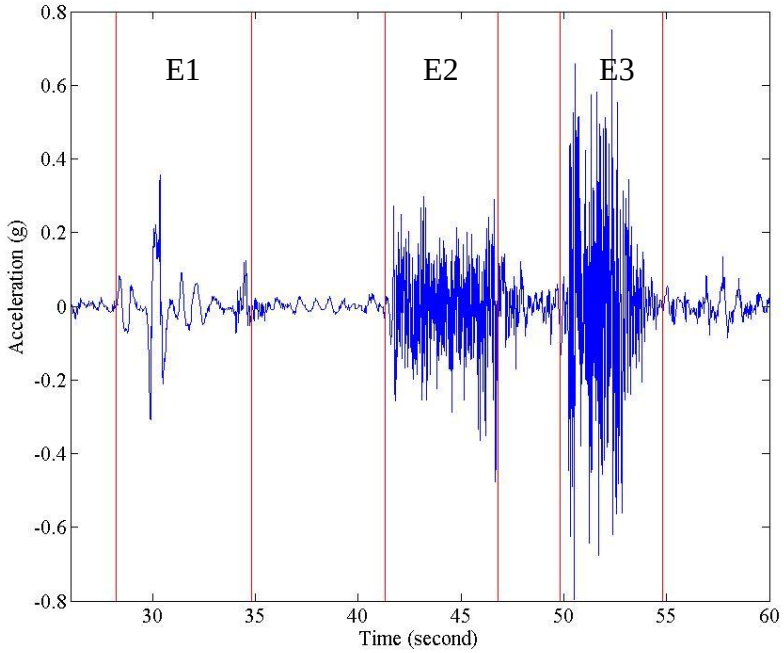

Figure 4.4: Separated three events using the acceleration data from the 1st counter-clockwise lap in Z direction

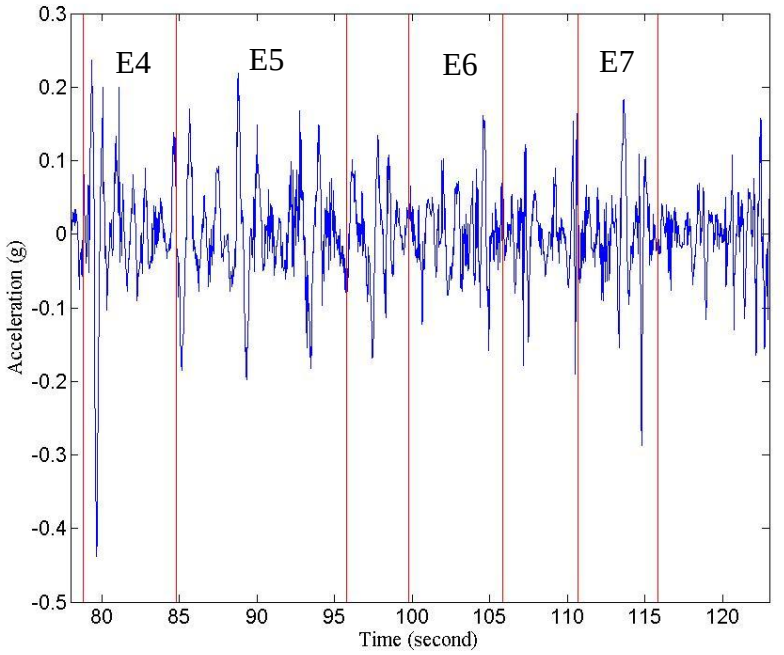

Figure 4.5: Separated four events using the acceleration data from the 1st counter-clockwise lap in Z direction

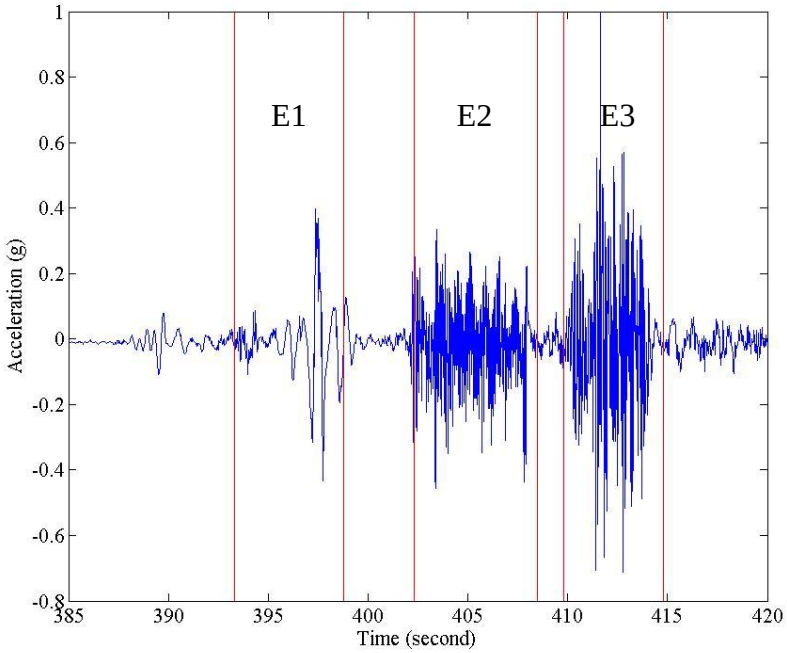

Figure 4.6: Separated three events using the acceleration data from the 1st clockwise lap in Z direction

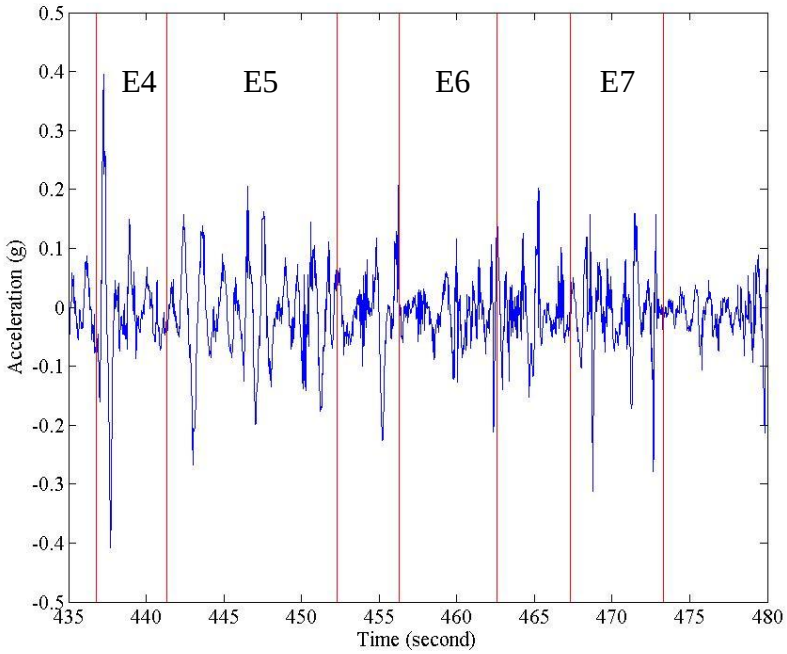

Figure 4.7: Separated four events using the acceleration data from the 1st counter-clockwise lap in Z direction

Referring to Figure 4.4 to Figure 4.7, based on the three and four events separation results using both of the counter-clockwise and the clockwise data, the accuracy of identified results can be demonstrated by comparing the identified events durations with those estimated based on the event geometry and driving speed. The identified three- and four- event durations, and the relative error determined with respect to the estimated ones using acceleration data from three counter-clockwise and three clockwise laps in X and Z directions, are summarized in Table 4.9 to Table 4.16:

Table 4.9: The identified three events durations compared with the estimated ones from three counter-clockwise laps in Z direction (The estimated durations of the three events are 5.79sec., 5.4 sec., and 3.5 sec., respectively.)

	1st Lap		2nd Lap		3rd Lap	
Event	Duration (s)	Relative error (%)	Duration (s)	Relative error (%)	Duration (s)	Relative error (%)
Event1	6	3.5	5.16	12.2	6	3.5
Event2	5.5	1.8	6.49	16.8	6.5	16.9
Event3	4.5	22.2	5.5	36.4	6.01	41.8

Table 4.10: The identified four events durations compared with the estimated ones from three counter-clockwise laps in Z direction (The estimated durations of the three events are 4.5sec., 10.3 sec., 3.4 sec., 6.7 sec., 3.5 sec., and 5.9 sec., respectively.)

	1st Lap		2nd Lap		3rd Lap	
Event	Duration (s)	Relative error (%)	Duration (s)	Relative error (%)	Duration (s)	Relative error (%)
Event 4	5	10	5.2	13.5	5.5	18.2
Event 5	10.5	1	11	5.5	10.5	1
Transition Bet E4 and E5	3.99	14.8	4	15	4	15
Event 6	6.51	2.9	7	4.3	6.5	3.1
Transition Bet E5 and E6	4.5	22.2	4	12.5	5	30
Event 7	5.5	7.3	6	1.7	5.5	7.3

Table 4.11: The identified three events durations compared with the estimated ones from three clockwise laps in Z direction

	1st Lap		2nd Lap		3rd Lap	
Event	Duration (s)	Relative error (%)	Duration (s)	Relative error (%)	Duration (s)	Relative error (%)
Event1	5.5	5.3	7	17.3	7.5	22.8
Event2	7.5	28	7.49	27.9	7	22.9
Event3	4.5	22.2	3.45	1.4	5	30

Table 4.12: The identified four events durations compared with the estimated ones from three clockwise laps in Z direction

	1st Lap		2nd Lap		3rd Lap	
Event	Duration (s)	Relative error (%)	Duration (s)	Relative error (%)	Duration (s)	Relative error (%)
Event 4	4.5	0	5.3	15.1	5.3	15.1
Event 5	11	6.4	10.5	1.9	11	6.4
Transition Bet E4 and E5	4	15	4.5	24.4	4	15
Event 6	6.3	6.3	6.5	3.1	6.5	3.1
Transition Bet E5 and E6	4.7	25.5	4.5	22.2	4	12.5
Event 7	6	1.7	6	1.7	5.2	13.5

Table 4.13: The identified three events durations compared with the estimated ones from three counter-clockwise laps in X direction

	1st Lap		2nd Lap		3rd Lap	
Event	Duration (s)	Relative error (%)	Duration (s)	Relative error (%)	Duration (s)	Relative error (%)
Event1	6	3.5	5	15.8	7	17.3
Event2	6	10	6	10	6.9	21.7
Event3	5.5	36.4	7.5	53.3	7	50

Table 4.14: The identified four events durations compared with the estimated ones from three counter-clockwise laps in X direction

Event	1st Lap		2nd Lap		3rd Lap	
	Duration (s)	Relative error (%)	Duration (s)	Relative error (%)	Duration (s)	Relative error (%)
Event 4	5.71	21.2	5	10	5.5	18.2
Event 5	10.5	1.9	10.5	1.9	8	28.8
Transition Bet E4 and E5	4	15	5	32	4.5	24.4
Event 6	6.5	3.1	5.5	21.8	6.5	3.1
Transition Bet E5 and E6	5	30	4.5	22.2	4	12.5
Event 7	6	1.7	5.5	7.3	5.2	13.5

Table 4.15: The identified three events durations compared with the estimated ones from three clockwise laps in X direction

Event	1st Lap		2nd Lap		3rd Lap	
	Duration (s)	Relative error (%)	Duration (s)	Relative error (%)	Duration (s)	Relative error (%)
Event1	5.5	5.3	5.4	7.2	6.5	10.9
Event2	6	10	5	8	6	10
Event3	4.5	22.2	3.43	2	4.9	28.6

Table 4.16: The identified four events durations compared with the estimated ones from three counter-clockwise laps in X direction

Event	1st Lap		2nd Lap		3rd Lap	
	Duration (s)	Relative error (%)	Duration (s)	Relative error (%)	Duration (s)	Relative error (%)
Event 4	5	10	5	10	4.8	6.2
Event 5	10.5	1.9	10.5	1.9	11.5	10.4
Transition Bet E4 and E5	4.5	24.4	4.5	24.4	3.5	2.9
Event 6	6.5	3.1	7	4.3	6.5	3.1
Transition Bet E5 and E6	4.5	22.2	4	12.5	5	30
Event 7	5.5	7.3	5.5	7.3	5	18

All the identified events durations are proved rigorously comparing with their estimated durations, as the percentage errors are relatively low. The percentage error is occasional high is expected due to the changing of the travelling speeds and the estimated error.

4.2 Mission Profile, Full-period PSD and Partial-period Driven Profile Generation of Accelerated Durability Test

In section 4.2.1, results of mission profiles consist of FDS and SRS of all the events are shown. In section 4.2.2, results of synthesized full 24 hours and 48 hours accelerated test PSD, FDS and ERS are presented, respectively; and they are further compared with the PSD, FDS and SRS of the field test. In section 4.2.3, the 60 seconds driven profiles of the partial-period test in a time series of the acceleration are generated using both of 24 hours and 48 hours PSD data. In section 4.2.4, the PSD, FDS and ERS of the partial-period accelerated test are generated based on the created 60 seconds acceleration data, and further compared with both of the full-period test and filed test to validate the partial test driven profiles. All the generated profiles used the acceleration data in both of the X and Z direction. In section 4.2.5, results of the parametric analysis are shown.

4.2.1 Results of Mission Profiles

The mission profiles of SRS generated using X and Z directions filed test acceleration data are shown in Figure 4.8, the horizontal axis is the frequency in the unit of Hz, and the veridical axis is the maximum shock response in the unit of g.

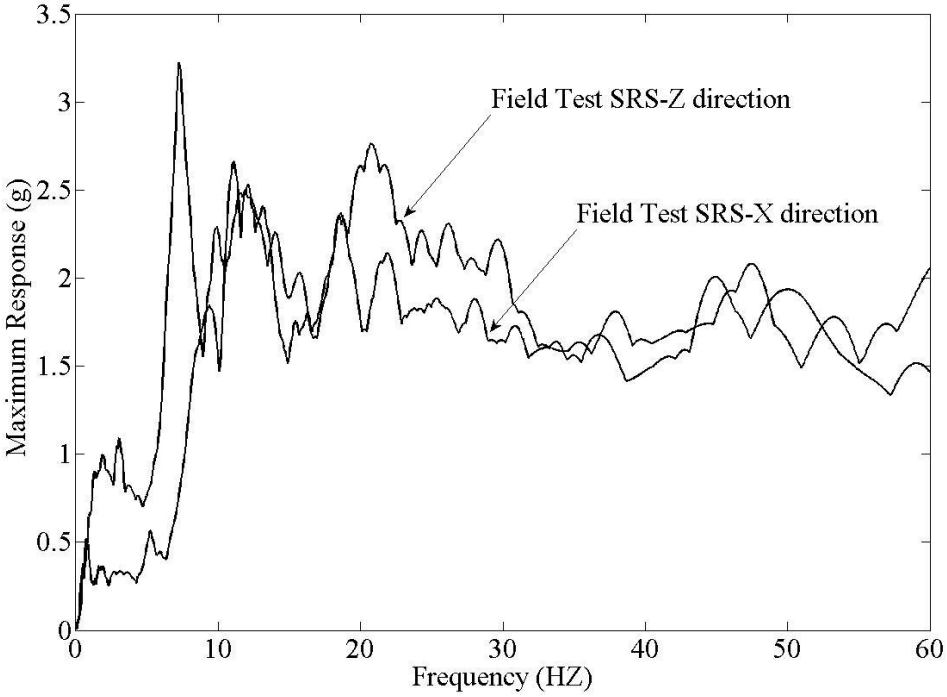

Figure 4.8: Field test SRS of X and Z directions

Referring to Figure 4.8, the generated field test SRS using acceleration data of X and Z directions have similar general trends albeit different magnitudes. The FDS generated using acceleration data of X and Z directions from the field test are shown in Figure 4.9, the horizontal axis is the frequency in the unit of HZ, and the veridical axis is the non-dimensional fatigue damage.

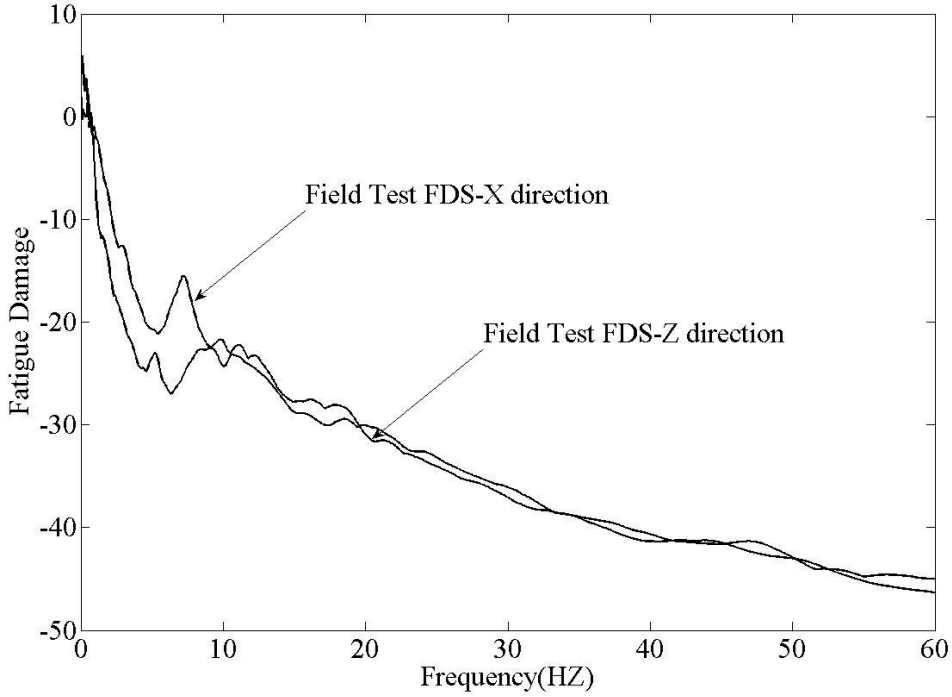

Figure 4.9: FDS for the field test loop of Z direction

Referring to Figure 4.9, the generated mission profiles FDS using X and Z directions have similar general trends albeit different magnitudes at each frequency. The important mission profiles of the field test SRS and FDS will be used to validate the full- and partial-period accelerated tests.

4.2.2 PSD Generation of Full-Period Accelerated Durability Test with respect to the Field Test

The generated 24 hours and 48 hours accelerated test PSDs and the original 330 hours field test PSD using the acceleration data in the X and Z directions are shown in Figure 4.10 and Figure 4.11:

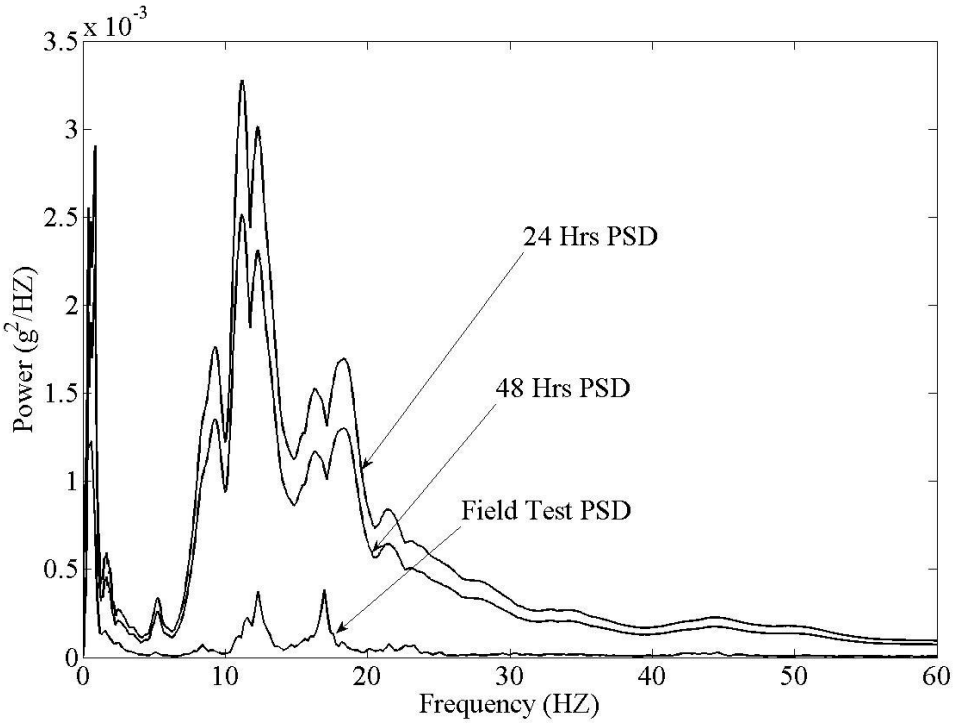

Figure 4.10: 24 hrs and 48 hrs accelerated test PSDs compared with the original field test PSD of X component

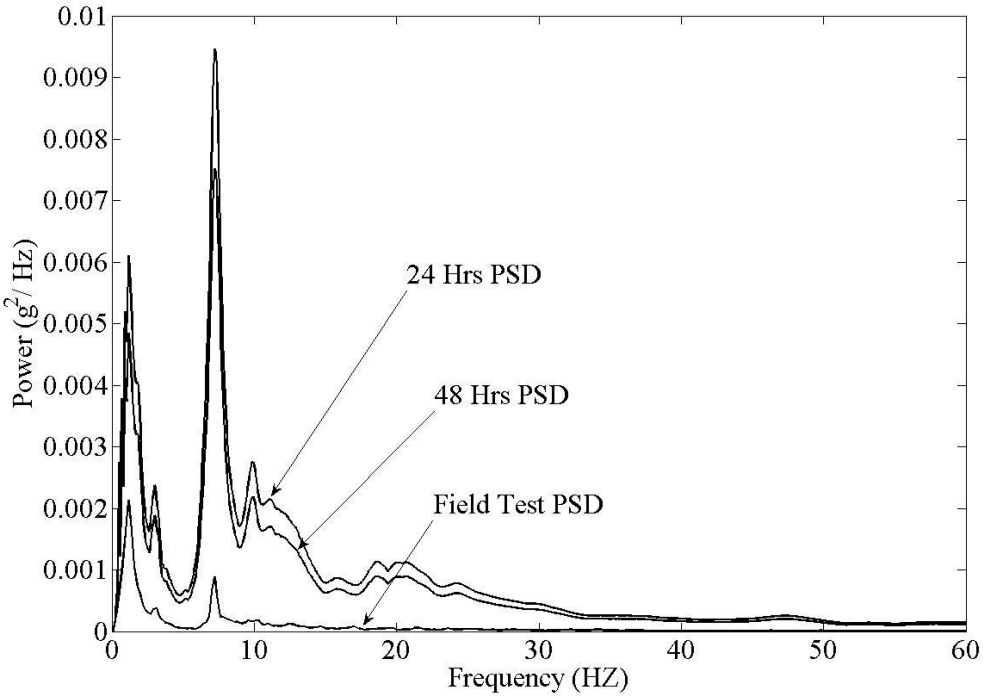

Figure 4.11: 24 hrs and 48 hrs accelerated test PSDs compared with the original field test PSD of Z component

Referring to Figure 4.10 to Figure 4.11, the 24 hours and 48 hours accelerated test PSDs have higher magnitudes than the original field test PSD, while keeping the same general trends. At the same time, the 24 hours accelerated test PSD has a general higher magnitude than the 48 hours accelerated test PSD. This is expected because the shorter the test period, the higher compression ratio for the PSD with respect to the field test is used. In addition, 1 Hz and 7 Hz are the important frequencies of the maximum power occurrence for Z direction data, however not for X direction data.

The generated 24 hours and 48 hours accelerated test FDS are compared with the original field test FDS respectively, as shown in Figure 4.12 and Figure 4.13:

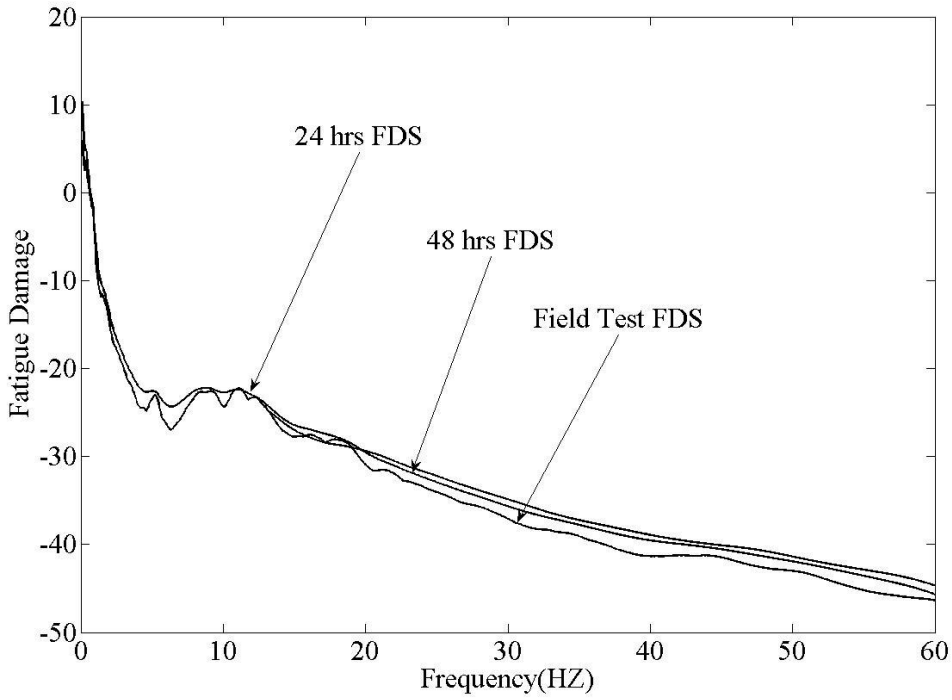

Figure 4.12: 24 hrs and 48 hrs accelerated test FDS compared with the field test FDS of X component

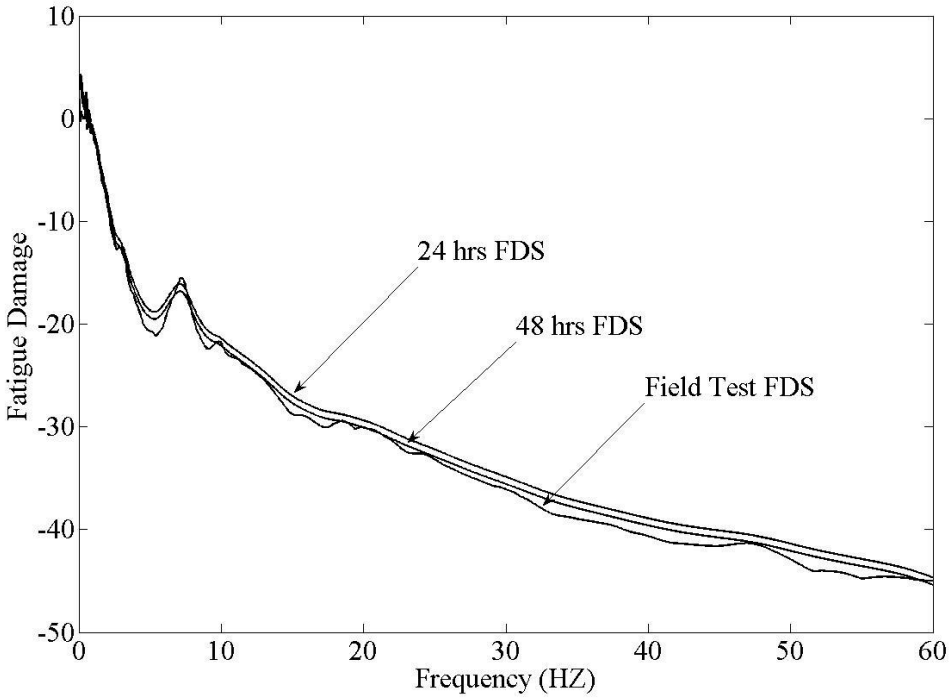

Figure 4.13: 24 hrs and 48 hrs accelerated test FDS compared with field test FDS of Z component

As Figure 4.12 and Figure 4.13 demonstrated, the magnitudes of the accelerated test FDS and the field test FDS are similar as they keep the same general trends, indicating there is likely no failure mechanism changes of the accelerated test with respect to the field test.

The 24 hours and 48 hours accelerated test ERS are generated and compared with the field test SRS respectively, as shown in Figure 4.14 and Figure 4.15:

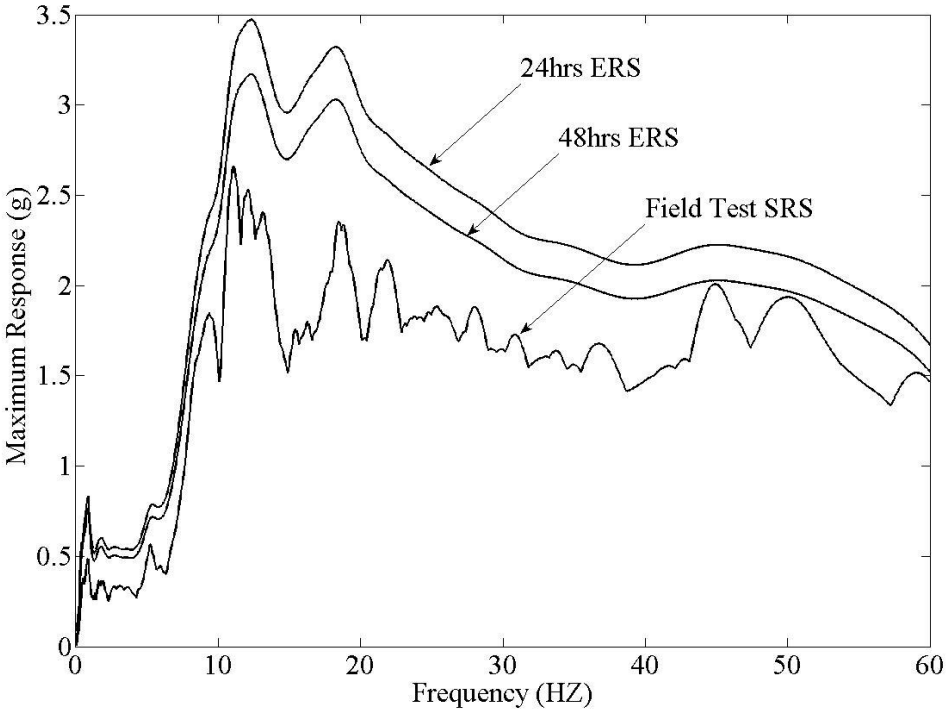

Figure 4.14: 24 hrs and 48 hrs accelerated test ERS compared with field test SRS of X component

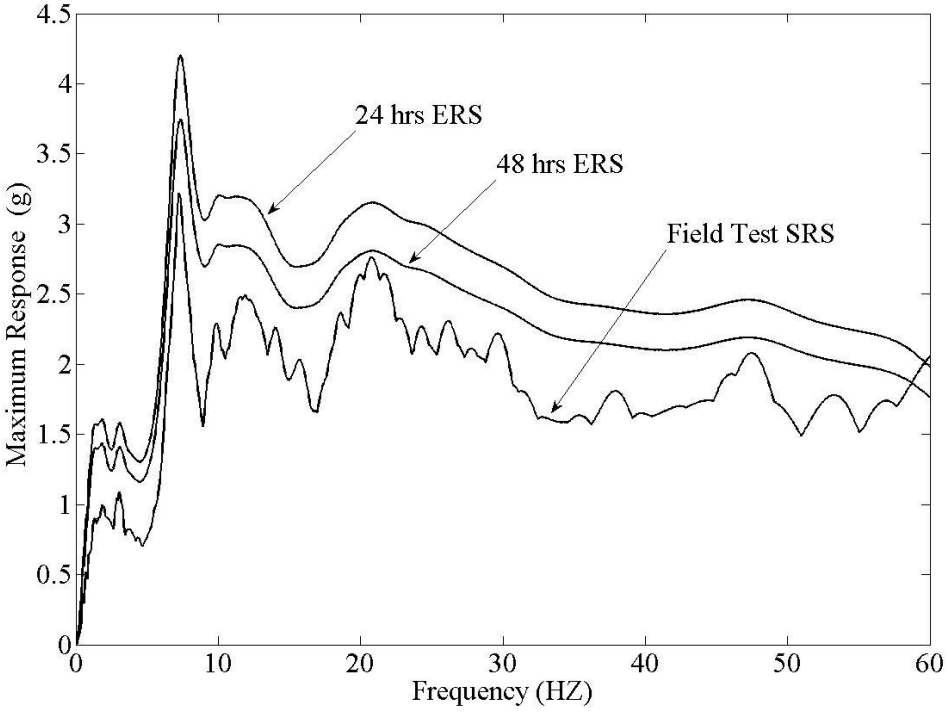

Figure 4.15: 24 hrs and 48 hrs accelerated test ERS compared with field test SRS of Z component

Referring to Figure 4.14 and Figure 4.15, the envelopes of the synthesized accelerated test ERS profile and the field test SRS profile keep the same general trends; however, the synthesized accelerated test ERS profiles are above the field test SRS profile, which does not satisfy the validation criteria for an accelerated test. More discussion will be presented in section 4.2.4.

4.2.3 Results of Partial Test Generation using a Random 60 seconds Time Series Driven Profile

The random 60 seconds driven profile of the partial-period test is generated from the created full-period test PSD data using Glyphworks software. The created 60 seconds acceleration data in terms of time series using the 24 hours and 48 hours PSDs data are shown respectively in Figure 4.16 and Figure 4.17:

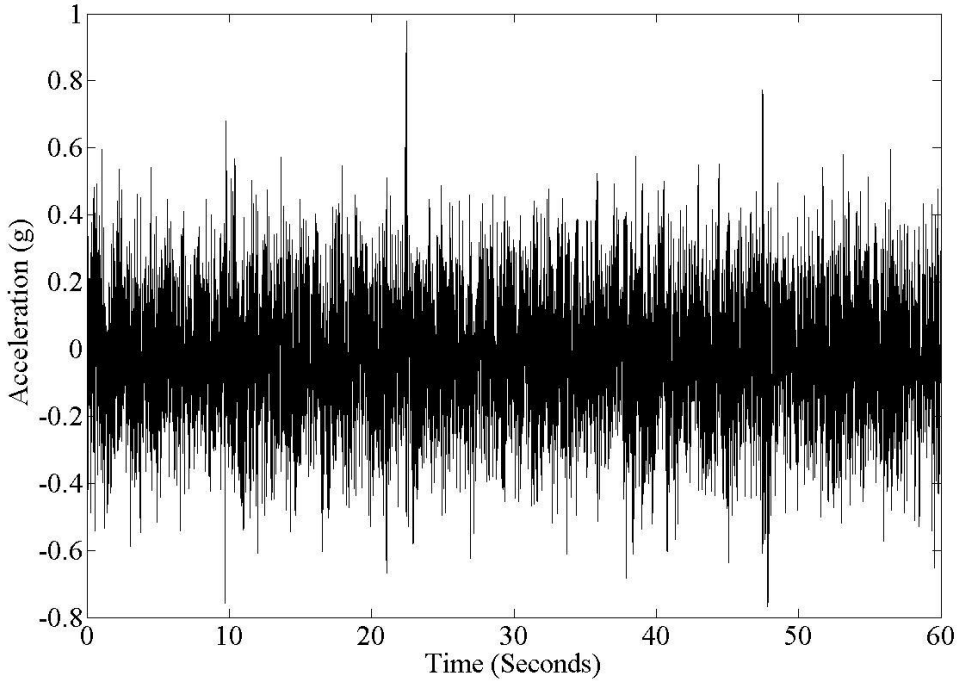

Figure 4.16: 60 seconds acceleration data generated by the 24 hrs PSD of Z component

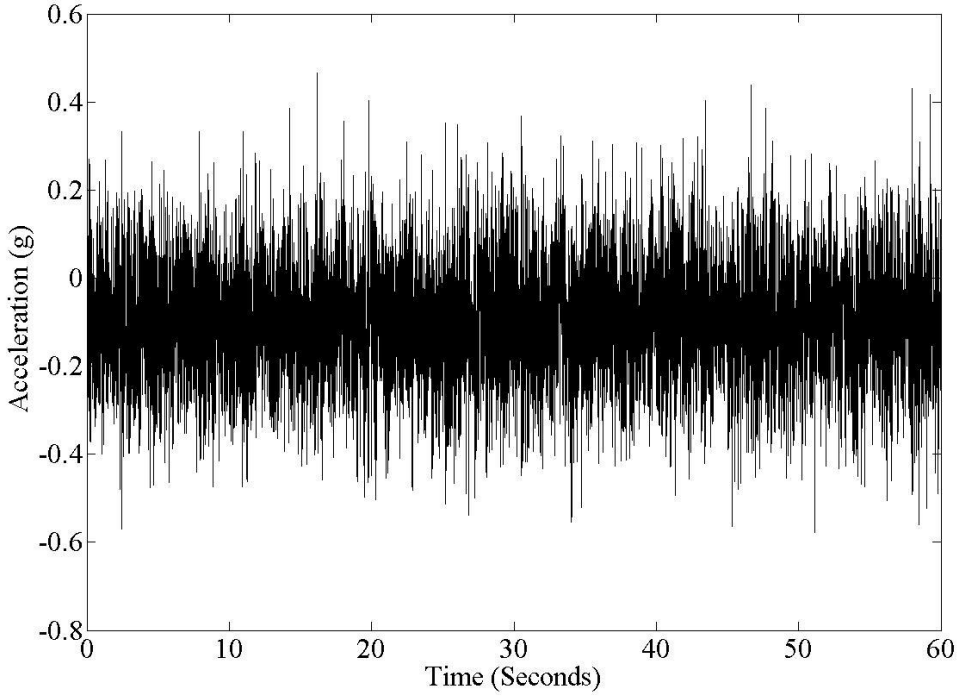

Figure 4.17: 60 seconds acceleration data generated by the 48 hrs PSD of Z component

Referring to Figure 4.16 and Figure 4.17, the generated 60 seconds acceleration data using both 24 hours and 48 hours accelerated test of Z direction have the same acceleration range. Meanwhile, the acceleration spikes at each time instance is different. The vibration for the sub-scaled accelerated test using 60 seconds driven profile generated via the 24 hours accelerated test PSD more severe is expected. Same results are determined using X direction data.

4.2.4 Results of Partial-period Test Validation using a Random 60 seconds Acceleration Driven Profile

The corresponding partial-period test PSD, FDS and ERS are generated using 60 seconds acceleration data; and they are further compared with PSD, ERS and SRS of full 24 hours and 48 hours test, and PSD, FDS and SRS of the field test, respectively as shown:

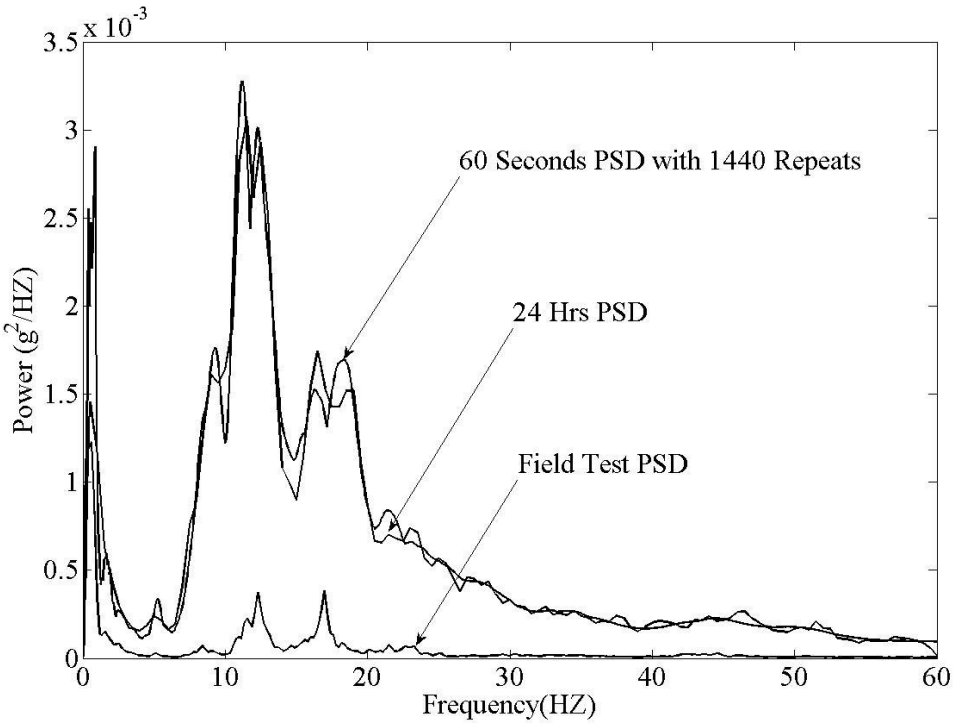

Figure 4.18: 60 seconds partial test PSD compared with 24 hours, and field test PSD of X component

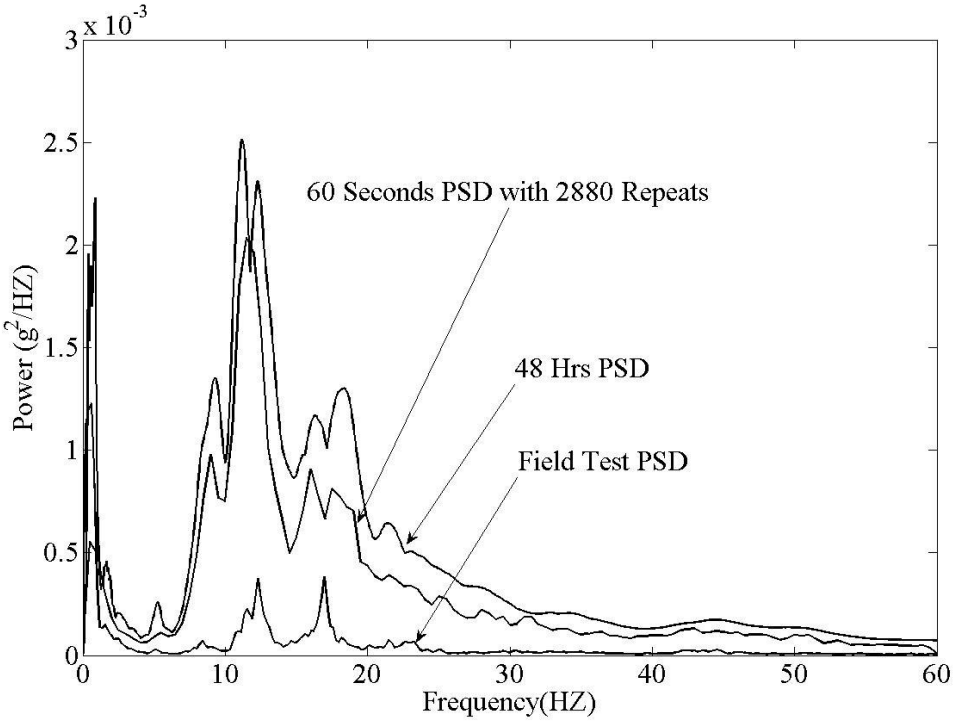

Figure 4.19: 60 seconds partial test PSD compared with 48 hours, and field test PSD of X component

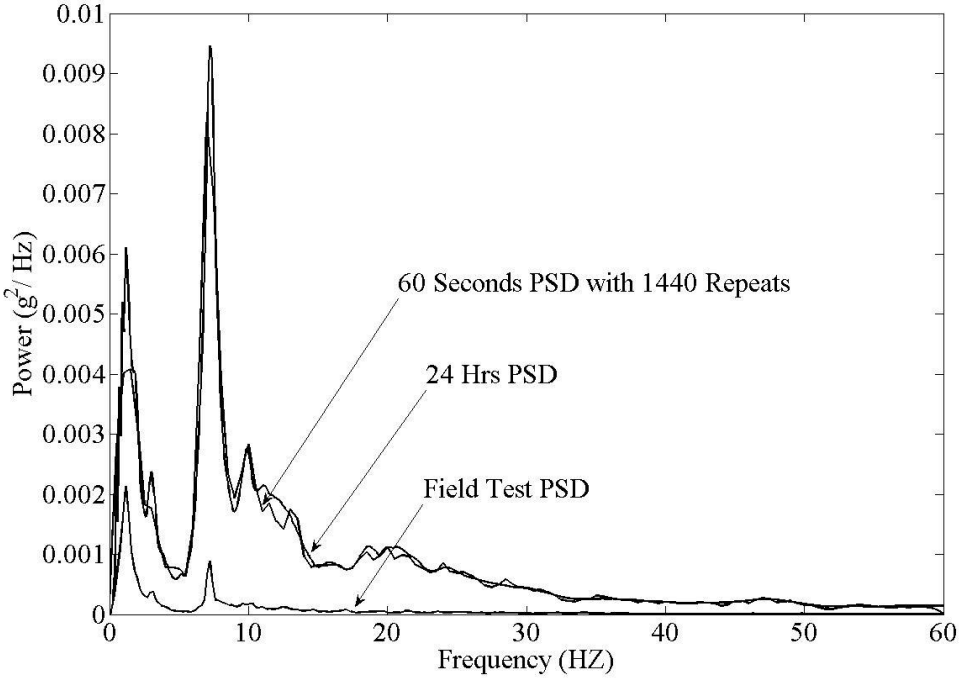

Figure 4.20: 60 seconds partial test PSD compared with 24 hours, and field test PSD of Z component

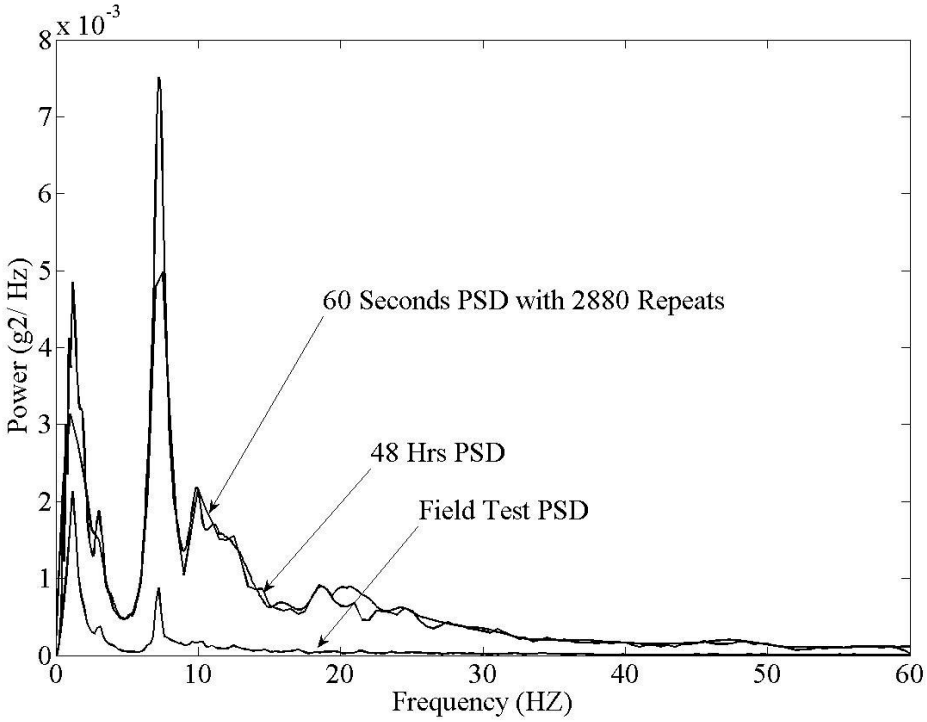

Figure 4.21: 60 seconds partial test PSD compared with 24 hours, and field test PSD of Z component

Referring to Figure 4.18 to Figure 4.21, the 60 seconds partial test PSD and the full-period test PSDs have the similar power magnitude, and they have higher magnitude than the PSD of the original field test.

The 60 seconds partial test FDS generated based on both of the 24 hours and 48 hours data are compared with the field test FDS, as shown:

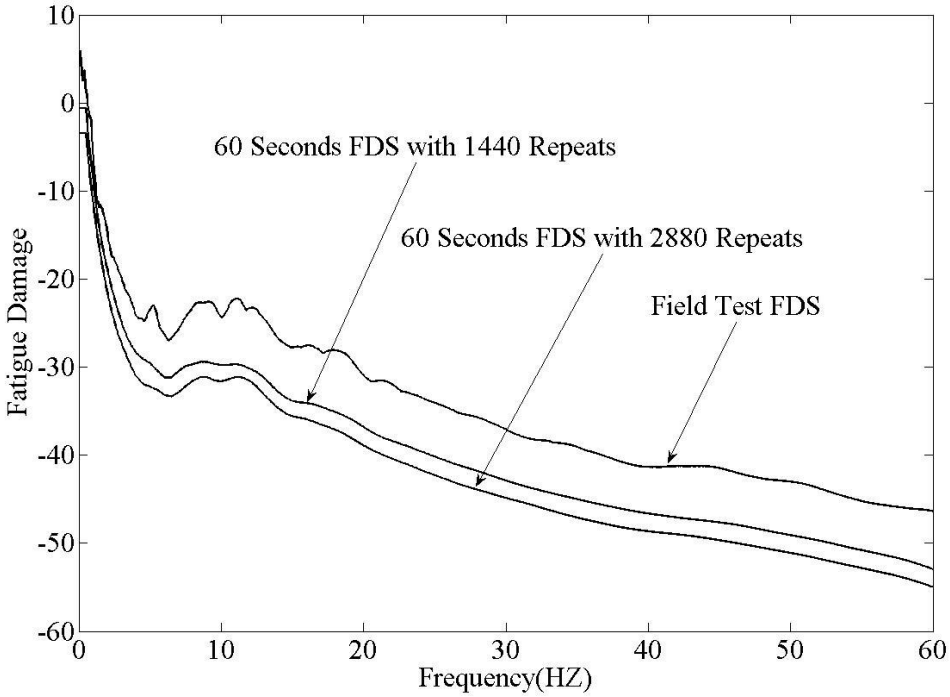

Figure 4.22: 60 seconds partial test FDS with 24 hrs repeats compared with field test FDS of X component

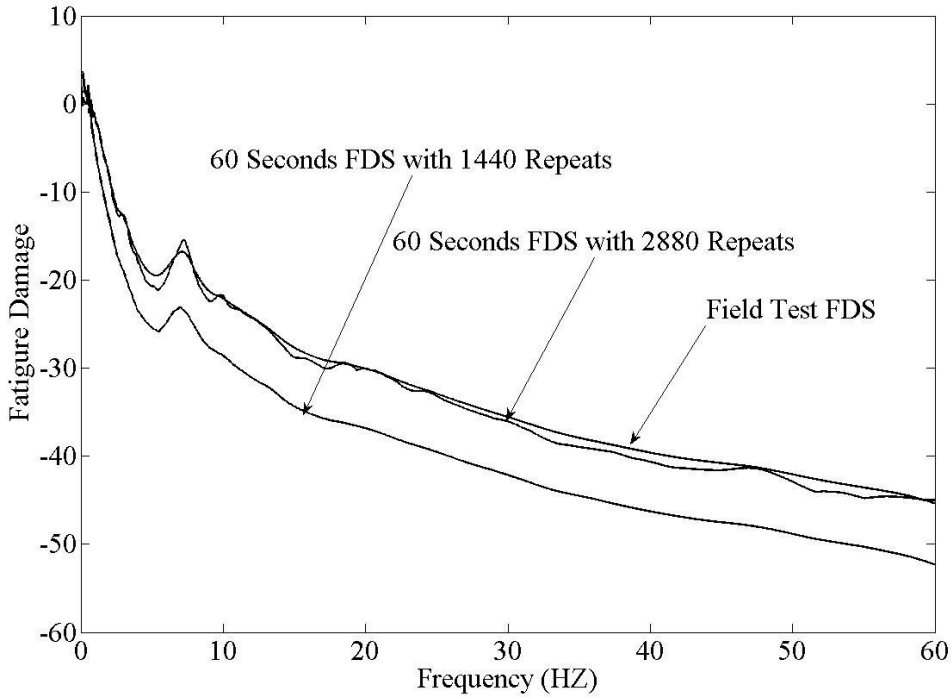

Figure 4.23: 60 seconds partial test FDS with 24 hrs and 48hrs repeats compared with field test FDS of Z component

As Figure 4.22 to Figure 4.23 demonstrated, the 60 seconds partial test FDS and field test FDS are similar in magnitudes while keep the same general trends. At the same time, the acclerated test FDS is lower than or equal to the field test FDS, which satify the validation critira.

The 60 seconds partial test ERS based on 24 hours and 48 hours data are generated and compared with field test SRS for both of the X and Z directions, as shown:

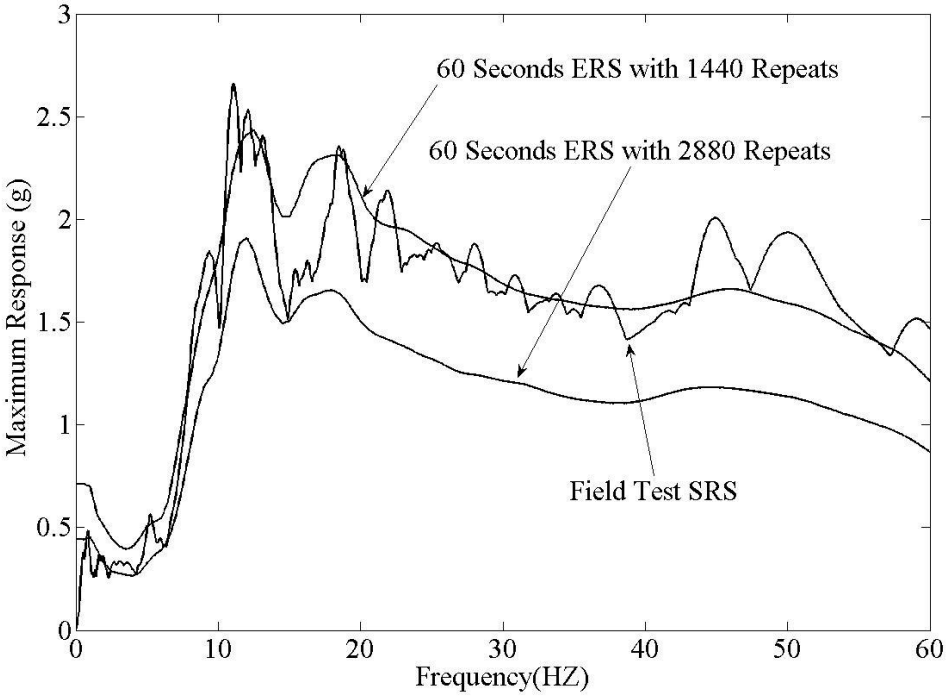

Figure 4.24: 60 seconds partial test ERS with 24 hrs and 48 hrs repeats compared with field test SRS of X component

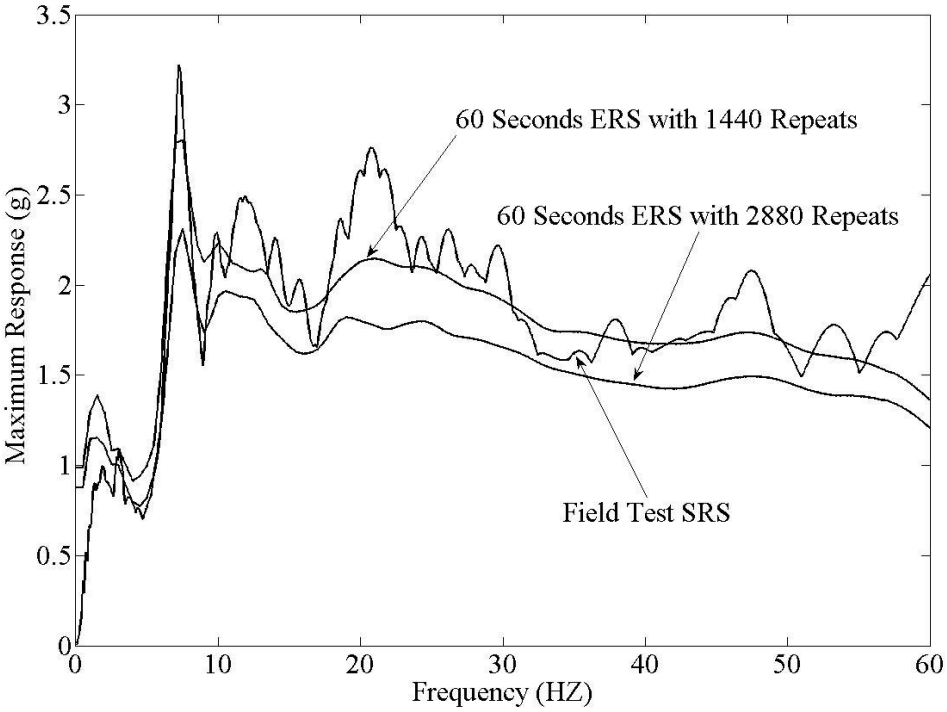

Figure 4.25: 60 seconds partial test ERS with 24 hrs and 48 hrs repeats compared with field test SRS of Z component

The envelope of the ERS profiles of the partial-period test and the SRS profile of the field test keep the same general trends; at the same time, the ERS profiles of the partial-period test are below the field test SRS profile, which satisfied the validation criteria for the partial test. Note that in Section 4.2.2, it was noticed that the profiles of ERS for the 24 hrs and 48 hrs durability tests are above the SRS profiles from the field test, which does not satisfy the validation criteria for an accelerated test in that the ERS profiles should not exceed those from the field test. However, since a loading profile with a significantly shorter partial-period (60 seconds) is required, some information is inevitably lost. As a result, the final resulted SRS from the partial-period loading profiles match those from the field tests.

4.2.5 Parametric Analysis

In this section, results of the parametric analysis on the important profiles, including the time durations, T_{test}, and fatigue parameter, b, on the partial-period test PSD generation**,** and fatigue parameter, b, on the partial-period test ERS and FDS generations are shown, respectively.

In order to examine the sensitivities of partial-period test PSD generation to the time durations, T_{test}, the acceleration data used as the loading profiles for 60 second, 3 minutes, and 5 minutes periods are generated. Their PSDs are compared with the full 24 hours accelerated test PSD, as shown in Figure 4.26:

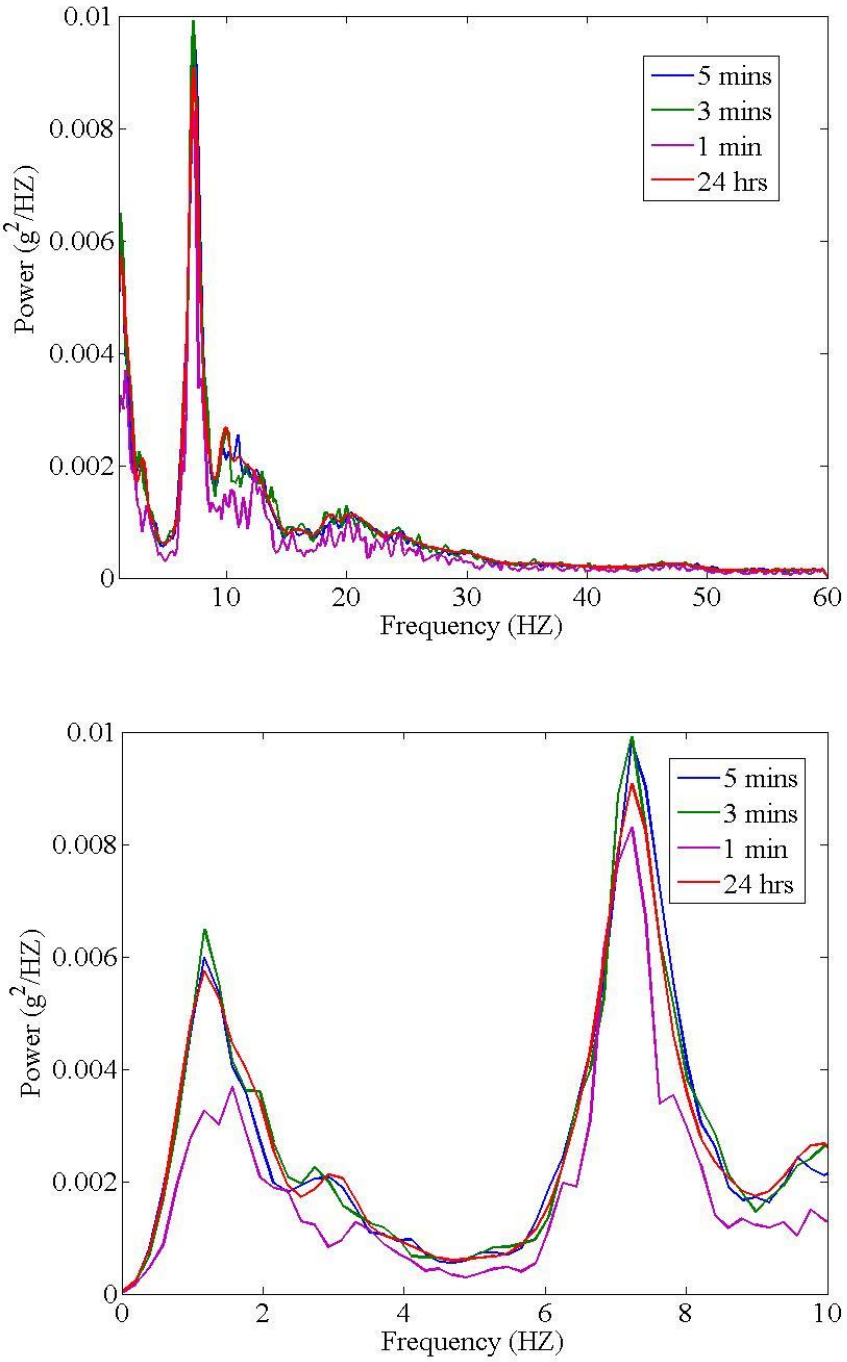

Figure 4.26: 60 seconds, 3 minutes and 5 minutes partial tests PSD compared with the full 24 hour accelerated test PSD (a) up to 60 HZ (b) up to 10 HZ

Referring to Figure 4.26 (a), the frequency and the power contents of the 60 seconds, 3 minutes, and 5 minutes partial tests are all consistent with the full 24 hours accelerated test, as they keep

the same general trends. Theoretically, important dynamic information contained in those partial-period test PSDs is compressed from the 24 hours accelerated test PSD.

In order to further examine the maximum power occurrence, 60 seconds, 3 minutes, 5 minutes and 24 hours PSDs of the partial test periods are plotted up to 10 HZ as shown in Figure 4.26 (b). The maximum powers of different partial-period tests conducted are occurred at frequency of 1HZ and 7HZ, indicating that the possibility of changes in failure mechanism of the testing vehicle for the partial-period tests with respect to the field test is low. In addition, at each frequency of the generated PSDs for the 3minutes and 5 minutes partial tests, the shorter T_{test} used for the partial test, a general higher magnitude of the power is resulted. For the 60 seconds partial test, powers are lost at important frequencies of 1Hz and 7Hz. However, there are many factors on the chosen of T_{test} for the partial tests, one of the main advantages to use 60 seconds partial test is the cost of tuning the actuators is low.

Another parametric analysis studied is on partial test PSD generation to the fatigue parameter, *b*. For 60 seconds partial test, PSDs are generated using values of *b* 2, 4, 6, and 8 in Equation 3.8, as shown in Figure 4.27:

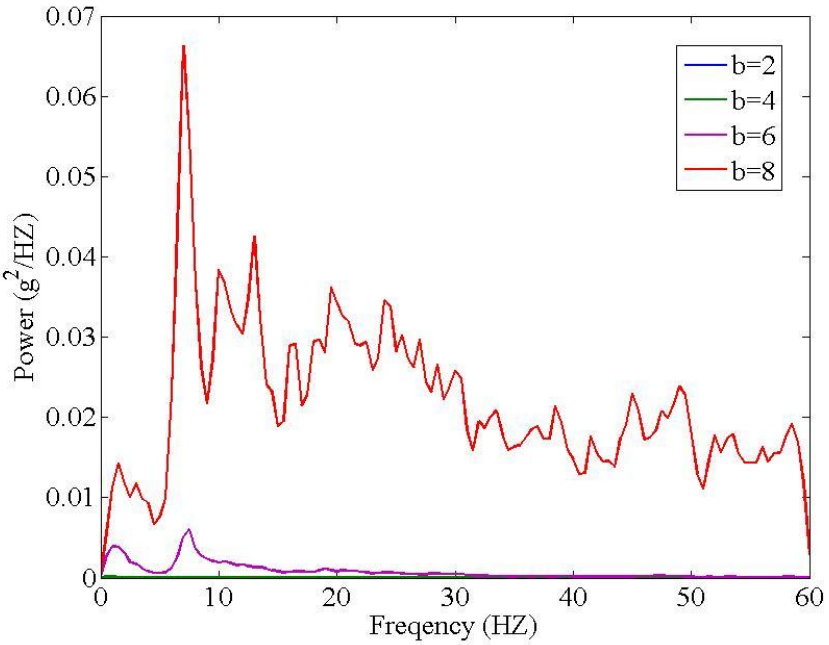

Figure 4.27: The partial-period test PSD profiles with different values of fatigue parameter

Referring to Figure 4.27, as the value of *b* increases the magnitude of the PSDs increases respectively with certain degrees. When *b* has a value of 2 or 4, the partial-period PSDs are relatively close to zero. Therefore, the higher *b* values result in the higher magnitude of the PSD profiles.

The last parametric analysis studied is on partial-period test ERS and FDS validation to the fatigue parameter, *b*. For 60 seconds partial test, ERSs are generated using different values of *b* 2, 4, 6, and 8, and they are plotted together with the field test SRS in Figure 4.28:

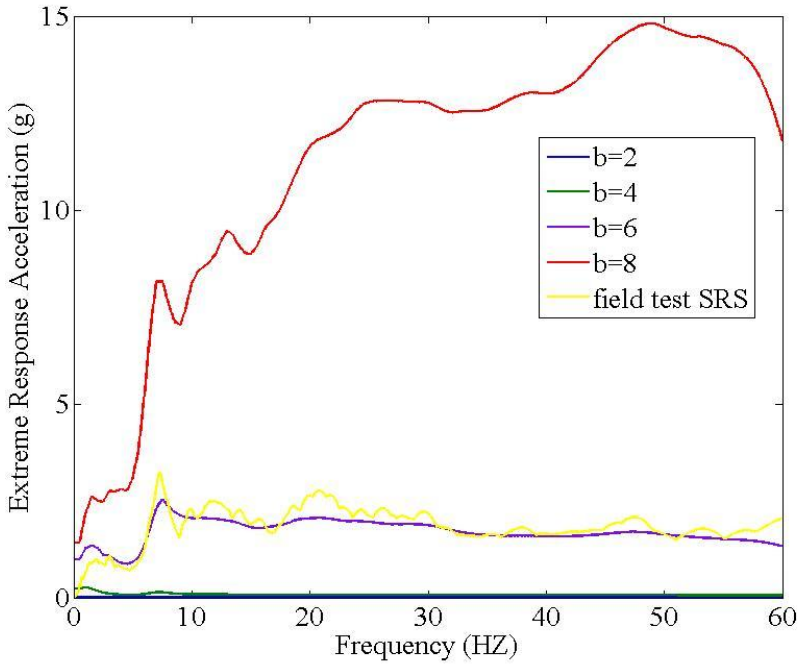

Figure 4.28: The partial-period test ERS profiles with different values of fatigue parameter

Referring to Figure 4.28, as the value of *b* increases the magnitude of the ERSs increases respectively. In addition, when *b* has a value of 8 the ERS of the partial test is above the SRS of the field test, which does not validate the partial test. When *b* has a value of 6, the ERS is equal to SRS of the field test; and when b has a value of 2 and 4, the ERS is below the SRS of the field test data, therefore, *b* values of 2, 4, 6 are acceptable for a validate partial test.

For 60 seconds partial test, FDSs are generated using different *b* values of 2, 4, 6, and 8, and they are plotted together with the field test FDS in Figure 4.29:

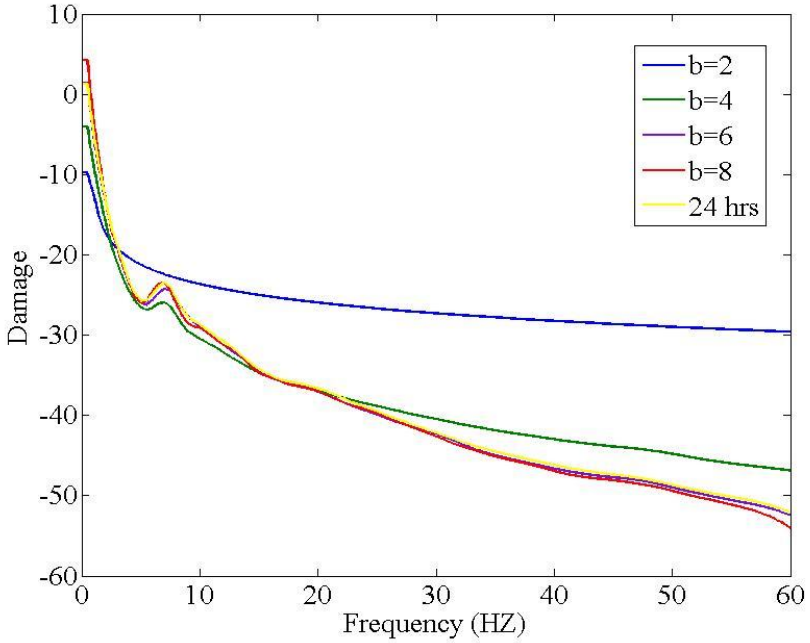

Figure 4.29: Different values of fatigue parameter, *b* 2,4,6,8 used for the partial-period test FDS generation

Referring to Figure 4.29, when *b* has a value of 4, 6 and 8, the magnitudes of the FDSs keep consistent at each natural frequency. When *b* has a value of 2, the FDS does not have the same general trends as the other ones. Therefore, *b* values of 4, 6, 8 are acceptable to validate a partial test.

According to the results shown on both Figure 4.28 and Figure 4.29, we conclude that *b* values of 2 and 8 are not acceptable; values of 4, 6 are acceptable. Therefore, for the future driven profile generation, values of 4, 6 can be selected for a valid partial test.

Chapter 5

Conclusions and Future Work

The accelerated durability test is important to quantify the life characteristics of ground vehicle components. The sub-scaled accelerated durability test is carried out on MAST. The driven profile generation for the MAST is an essential task, and it can be created by the commercial GlyphWorks software. In general, the mission profiles of the accelerated durability test can be generated via the acceleration data of the events experienced by the vehicle during the field test. The representative full-period test PSD profile can be generated based on the mission profiles. Then, the partial-period acceleration data, i.e., the driven profile for the sub-scaled accelerated durability test can be generated based on the full-period test PSD data. Therefore, to accurately separate the acceleration data that correlates the load events becomes essential to efficiently generate the mission profiles for the accelerated test analysis. In addition, to successfully generate the mission profiles, full-period test PSD profile are essential for the partial-period driven profile creation of the sub-scaled accelerated durability test.

Methods for the automatic events identification including the designed clustering based algorithm and the Fourier boundary refinement method using the wavelet denoised signal have been developed. The methods are shown to be efficient and accurate with the real field test data. In addition, the identified events for the counter-clockwise laps are just as good as the clockwise laps with the proposed methods.

The mission profiles and the full-period accelerated test PSD for the durability test are successfully generated using GlyphWorks from those accurately identified events times. Consequently driven profiles for the test with partial-period loading is successfully generated based on the PSD data for the full-period test. In addition, systematic approaches to generate and to validate the partial-period test driven profiles have been successfully developed. Parameters of the testing duration, T_{test} and the fatigue parameter, b on the efficient generation of partial-period test PSD have been investigated; both of them have effects on the magnitude of the PSD data. Adequate fatigue parameter, b for the generation of ERS and FDS have been successfully determined to obtain a valid partial-period durability test. Therefore, the accelerated durability test can be further conducted in the mechanics lab using the time series format driven profile.

Further improvements need to be made in future work. First, the new designed clustering algorithm is used for seven events identification in this work. When different field test data is collected, the programs of the designed clustering algorithm in Matlab need to be modified according to the number of the clusters embedded. In addition, the optimum threshold values may have to be modified as well, depending on the signal patterns. Furthermore, in this work, the envelope of full-period test ERS exceeds the one of SRS from the field test. However, due to the short duration of the loading profile for the partial-period test, the SRS from the partial-period durability tests is close to the one form the field tests. Further experimental research is recommended to investigate the effectiveness of the proposed loading profiles for the partial-period durability tests.

References

[1] GlyphWorks Worked Examples 5.1 [Electronic], Available with nCode GlyphWorks software, Ncode, 2007.

[2] S. Cull, C. Yang, and C. Wu, "Generation and verification of accelerated durability tests", Department of Mechanical and Manufacturing Engineering, University of Manitoba, Internal Report, 2010.

[3] Western Canada testing Inc. (Feb, 2008). "Westest's MAST Table" [Online]. Available: http://www.westest.ca/mast.htm [August 16, 2009]

[4] Pennsylvania Transportation Institute-Vehicle System and Safety Group. (Nov, 2007). "Bus Research and Testing Facility Test Track" [Online]. Available: http://www.vss.psu.edu/BTRC/btrc_test_track.htm [August 16, 2010].

[5] Cheng-Ping Lai, Pau-Choo Chung, Vincent S. Tseng, "Expert System with Applications", *An international Journal*, vol.37, pp.6319-6326, 2010.

[6] S. Cull, K. Xu, and C. Wu, "Generating accelerated loading profiles from measured time series data", Department of Mechanical and Manufacturing Engineering, University of Manitoba, Internal Report, 2009.

[7] P. Zhang and C. Wu, "Events identification of curve fitting method", Department of Mechanical and Manufacturing Engineering, University of Manitoba, Internal Report, 2010.

[8] Bartosz Kozlowski, "Time series denosing with wavelet transform", *Journal of Telecommunications and Information Technology*, pp. 91-95, 2005.

[9] Junhui Qian, "Denosing by wavelet transform", Rice University, Department of Electrical Engineering.

[10] M. Misiti, Y. Misiti, G. Oppenheim, J. M. Poggi, Wavelet toolbox user's guide, The MathWorks, 1996.

[11] I. Y. Soon, S. N. Koh, C. K. Yeo, "Wavelet for Speech Denoising", *Speech and Image Technologies for Computing and Telecommunications, Proceeding of IEEE,* Brisbane, QLD, pp. 479-482, 1997.

[12] Rui. Xu, Donald. C. Wunsch, Clustering, IEEE Press Series on Computational Intelligence, 2009.

[13] Backer, E. and Jain, A. "A clustering performance measure based on fuzzy set decomposition", *IEEE Transactions on Pattern Analysis and Machine Intelligence*, vol.3 (1), pp. 66-75, 1981.

[14] T. Warren. Liao, "Clustering of time series data-a survey", *The Journal of the Pattern Recognition Society*, vol.38, pp.1857-1874, 2005.

[15] H. Olkkonen, "Running discrete Fourier transform for time-frequency analysis of biomedical signals", vol.17 (6), pp.455-458, 1995.

[16] L. Gelman, M. Sanderson, C. Thompson, "Signal recognition: Fourier transform vs. Cosine trsnform", *The Journal of the Pattern Recognition Letters*, vol.24, pp.2823-2827, 2003.

[17] Ervin. Sejdi´c, Igor. Djurovi´c, Jin. Jiang, "Time–frequency feature representation using energy concentration: An overview of recent advances", *The Journal of the Digital Signal Processing*, vol.19, pp.153-183, 2009.

[18] Ervin. Sejdic´, Igor. Djurovic, LJubiˇsa. Stankovic, "Fractional Fourier transform as a signal processing tool: An overview of recent developments", *The Journal of the Signal Processing.* vol.91 (6), pp.1351-1369, 2010.

[19] L.Kaur, S. Gupta, R. C. Chauhan, "Image denoising using wavelet thresholding", Avilable: http://www.ee.iitb.ac.in/~icvgip/PAPERS/202.pdf

[20] Michel. Misiti, Yves. Misiti, Georges. Oppenherim, Jean-Michel. Poggi. *Wavelet toolbox user's guide*, Available: http://web.mit.edu/1.130/WebDocs/wavelet_ug.pdf. 1996.

[21] S. Tsai, *"Wavelet Transform and Denoising"*, Master's Thesis, URN: etd-12062002-152858, Chapter 4, pp. 35-42.

[22] A. Lallouani, M. Gabrea, C. S. Gargour, "Wavelet based speech enhancement using two different threshold-based denoising algorithms", *Canadian Conference on Electrical and Computer Engineering*, Ontario, pp. 315-318, 2004.

[23] Albert. Boggess, Francis J. Narcowich. *A first course in Wavelets with Fourier Analysis*. Prentice Hall, 2001.

[24] Robert J. Barsanti, "Wavelet noise removal from baseband digital signals in bandlimited channels", Available: http://ece.citadel.edu/barsanti/Research/barsanti_ssst2010_68_final.pdf.

[25] R. J. Barsanti, M. P. Fargues, "Wavelet based denosing of acoustic transients", *thirtieth Asilomar conference on Signal, System and Computers*, Pacific Grove, CA, pp 848-852, 1996.

[26] Lan. Xu, Hon. Keung. Kwan, "Adaptive wavelet denosing system for speech enhancement," *International Symposium on Circuits and Systems, proceeding of IEEE,* Seattle, WA, pp 3210-3213, 2008.

[27] Yan. Wu, A universal interpolative filter for low-pass and bandpass signal-CSINC interpolator, *Digital Signal Processing*, vol.15 (5), pp.425-6426, 2005.

[28] "Methods of Clustering and Fourier analysis," Class notes for MATH 7890 Directed Study in Applied Mathematics, Department of Mathematical Science, University of Georgia Southern University, 2010.

[29] K. Xu, and C. Wu, "Generating accelerated loading profiles for motor coaches", Undergraduate Thesis, Department of Mechanical and Manufacturing Engineering, University of Manitoba, Winnipeg, MB, 2009.

[30] Cheng-Ping Lai, Pau-Choo Chung, and Vincent S. Yseng, A novel two–level clustering method for time series analysis, Expert *Systems with Applications*, vol. 37, pp 6319-6326, 2010.

[31] G. Gan, C. Ma, and J. Wu, Data Clustering Theory, Algorithms, and Applications, ASA-SIAM series on statistics and applied probability, Philadelphia, PA, 2007.

[32] Y. Wu, A universal interpolative filter for low-pass and bandpass signal-CSINC interpolator, *Digital Signal Processing*, vol. 15, pp. 425-436, 2005.

[33] T. W. Liao, Clustering of time series data-a survey, *The Journal of the Pattern Recognition Society*, vol. 38, pp. 1857-1874.

[34] Lioing. Deng, John. G. Harris, "Wavelet Denosing of Chirp-like Signal in the Fourier Domain", *IEEE International Symposium on Circuits and Systems*, Orlando, FL, pp 540-543, 1999.

[35] H.G.R. Tan, A. C. Tan, P. Y. Khong, V. H. Mok, " Best Wavelet Function Identification System for ECG signal Denoise Applications", *International Conference on Intelligent and Advanced Systems,* Kuala Lumpur, pp. 631-634, 2007.

[36] A. Saha, R. P. Chatterjee, U. Dutta, "Motion Control of Snake Robot by Lead-Lag Compensator Designed with Frequency Domain Approach", *Proceedings of the 9th WSEAS International Conference on Robotics, Control and Manufacturing Technology*, Stevens Point, Wisconsin, pp. 13-20, 2009.

[37] D. L. Donoho, "De-Noising by Soft-Thresholding", *IEEE transactions on Information Theory,* vol.41 (3), pp.613-627, 1995.

[38] S. G. Chang, B. Yu, M. Vetterli, "Adaptive Wavelet Thresholding for Image Denosing and Compression", *IEEE Transaction on Image Processing,* vol.9 (9), pp.1532-1546, 2000.

[39] Hongwei. Guo, Yanchi. Liu, Helan Liang, Xuedong. Gao, "An application on time series clustering based on wavelet decomposition and denoising", *Fourth International Conference on Natural Conputation*, Jinan, China, 2008.

[40] Yan. Wu, "Linear subband predictive filters for wideband signals", *proceedings of the 5th WSES int. Conf. on Circuits, Systems, Electronics, Control & Signal Processing*, Dallas, USA, 2006.

[41] A. M. Alonso, J. R. Berrendero, A. Hernandez, A. Justel, "Time series clustering based on forecast densities", *Computational Statistics & Data Analysis*, vol.51, pp.762-776, 2006.

[42] Soon H. Kwon, "Threshold selection based on cluster analysis", *Pattern Recognition Letters*, vol.25, pp.1045-1050, 2004.

[42] Xiaoming. Jin, Yuchang. Lu, Chunyi. Shi, "Cluster time series based on partial information", *International Conference on System, Man and Cybernetics*, Hammamet, Tunisia, 2002.

[43] Fusheng. Yu, Keqiang Dong, Fei. Chen, Yongke. Jiang, Wenyi. Zeng, "Clustering time series with granular dynamic time warping method", *IEEE International Conference on Granular Computing*, California, USA, 2007.

[44] L. Karamitopoulos, G. Evangelidid, "Cluster-based similarity search in time series", Fourth Balkan conference in Informatics, Thessalonili, Greece, 2009.

[45] S.C. Ashmore, A. G. Piersol, J. J. Witte, "Accelerated service life testing of automotive vehicles on a test course", *Vehicle Dynamics*, vol.21, pp. 89-108, 1995.

[46] H. Haga, "evaluation of tyre models for durability loads prediction using a suspension-on-a-drum environment", *Vehicle System Dynamics*, vol.43, pp. 2819-296, 2005.

[47] N. Wilson, H. Wu, H. Tournay, C. Urban, "Effects of wheel/rail contact patterns and vehicle parameters on lateral stability", *Vehicle System Dynamics*, vol.48, pp. 487-503, 2010.

[48] M. Ansari , E.Esmailzadeh , D.Younesian, "Frequency analysis of finite beams on nonlinear Kelvin–Voight foundation under moving loads", *Journal of Sound and Vibration*, vol.330, pp. 1455-1471, 2011.

[49] J. Wannenburg, P.S. Heyns, "An overview of numerical methodologies for durability assessment", *International Journal of Vehicle Systems Modelling and Testing*, vol.5, pp. 72-101, 2010.

[50] D. Benasciutti, R. Tovo, "Spectral methods for lifetime prediction under wide-band stationary random processes", *International Journal of Fatigue*, vol.27, pp. 867-877, 2005.

[51] S. Bruni, M. Bocciolone, S. Beretta, "Simulation of bridge-heavy road vehicle interaction and assessment of structure durability", *Heavy Vehicle Systems, Int.J. of Vehicle Design*, vol.10 nos. 1/2, pp. 70-89, 2003.

[52] A. Lutz, J. Rauh, W. Reinalter, "Developments in vehicle dynamics and the tire model performance test", *Vehicle Systems Dynamics*, vol.45, pp. 7-19, 2007.

[53] S. Srikantan, S. Yerrapalli, H. Keshtkar, "Durability design process for truck body structure", *International Journal of Vehicle Design*, vol.23, pp. 94-108, 2000.

[54] A. Beevers, "Durability testing and life prediction of adhesive joints", *International Journal of Material and Product Technology*, vol.14, pp. 373-384, 1999.

[55] Specification Development using ERS and FDS, Available: http://christian.lalanne.free.fr/Home/Home_E.htm, 2009.

[56] K. BOGSJÖ, "Development of analysis tools and stochastic models of road profiles regarding their influence on heavy vehicle fatigue", *Vehicle System Dynamics*, vol.44, pp. 780-790, 2006.

[57] B. D. Youn, K. K. Choi, J. Tang, "Structural durability design optimization and its reliability assessment", *International Journal of Product Development*, vol.1 nos. 3/4, pp. 383-401, 2005.

[58] Peijun. Xu, "A technique for developing a high accuracy durability test for a Light Truck on a Six Degree-of Freedom Road Test Simulator", *International Journal of Vehicle Design*, vol.47 nos. 1/2/3/4, pp. 290-304, 2008.

[59] "An introduction to Muti-Axis Simulation Tables (MAST)", Slides from MITACS.

[60] "Appling Technology for Industry", Slides from MITACS.

[61] K. Dressler, M. Speckert, and G. Bitsch. "Virtual durability test rigs for automotive engineering", *Vehicle System Dynamics*. vol. 47 (4) April 2009, 387-401

[62] Gopalakrishnan, R. and Agrawal, H.N. "Durability analysis of full automotive body structures", *International Congress & Exposition*, 1993.

[63] J.Wannenburg, and P. S. Heyns. "An overview of numerical methodologies for durability assessment of vehicle and transport structures", *Int. J. Vehicle Systems Modeling and Testing,* vol. 5(1), 2010.

[64] Peijun Xu. "A technique for developing a high accuracy durability test for a Light Track on a Six Defree-of-Freedom Road Test Simulator", *Int. J. Vehicle Design*, Vol. 47, Nos. 1/2/3/4, 2008.

[65] Dressler, K. and Kottgen, "V.B. Synthesis of realistic loading specifications", *European journal of Mechnical Engineering,* vol. 41(3), 1999.

[66] Bannantine, J. A., Comer, J.J. and Handrock, J.L. Fundamentals of Metal Fatigue Analysis. New Jersey: Pretice-Hall, 1990.

[67] Cherng, J., Goktan, A., French, M., Gu, Y. and Jacob, "Improving drive files for vehicle road simulations", *Mechanical Systems and Signal Processing*, vol. 15(5), pp.1007-1022, 2001.